

Chapter

Asymptotic Solutions for Multi-Hole Problems: Plane Strain versus Plane Stress Boundary Conditions in Borehole Applications

Manal Alotaibi and Ruud Weijermars

Abstract

The elastic response of circular cylindrical holes in elastic plates is analyzed using the linear superposition method (LSM) to assess the impact of plate thickness on the stress state for the thin- and thick-plate solutions. Analytical solutions for stress accumulations near holes in elastic plates are relevant for a wide range of practical applications. For example, detailed analyses of the stress concentrations near boreholes piercing rock formations are needed during drilling operations to avoid premature fracturing due to tensile and shear failure. Stress concentrations near tiny holes in very thick plates approach the solution of a plane strain boundary condition; for large holes in very thin plates, the solution of a plane stress boundary condition will apply. For most practical cases, the response will be intermediate between the plane stress and plane strain end members, depending on the relative dimensions of the thickness of the elastic volume penetrated and the hole diameter. A nondimensional scaling parameter is introduced to quantify for which hole radius to plate thickness ratio occurs the transition between the two types of solutions (plane strain versus plane stress). Moreover, in this study, we consider the case of the presence of the internal pressure load in the analysis of the stress concentrations near boreholes. This consideration is important to carefully assess the magnitude of the elastic stress concentrations and their orientation near the hole in the rock formation when the pressure load of the mud is added to the borehole during drilling operations. For holes subjected to an internal pressure only, there is no difference between the plane stress (thin-plate solution) and plane strain solutions (thick-plate solutions). For cases with far-field stress, the plane strain solution is more sensitive to the Poisson's ratio than the plane stress solution. Multi-hole problems are also evaluated with LSM and the results are benchmarked against known solutions of different methods.

Keywords: displacement fields, linear superposition method (LSM), multi-hole solutions, plane strain, plane stress

1. Introduction

This study seeks to clarify the accuracy and possible limitations of the classical analytical solutions of Kirsch [1]—for the stress tensor field in linear-elastic plates pierced by one or more circular holes under certain far-field stress and internal pressure loads—when used in practical applications. These solutions are widely applied in wellbore-stability models and tunneling applications, and regularly involve the superposition of elastic displacements due to various boundary forces (far-field and internal pressure-loading) acting on the holes. Such situations have been systematically evaluated for linear-elastic isotropic and anisotropic rocks under a plane stress assumption [2–4].

However, recurrent concerns prevail related to the accuracy of results when using the solutions of [1] without modifications in wellbore-stability models. For example, the density of drilling mud pumped into the space between the wellbore and the drill string during drilling operations needs to be selected such that fracturing due to tensile and shear failure will not occur [5–7]. Obviously, the magnitude of the elastic stress concentrations and their orientation near the hole in the rock formation will rapidly vary when the pressure load of the mud is added to the borehole. When there is no internal pressure on the wellbore, the stress concentration factor for uni-axial far-field stress is always 3 (and for a biaxial compression reaches 4 [8]). However, when a net pressure is exerted on the wellbore's interior, the induced elastic deformation of the host rock increases or decreases the stress concentrations induced by the far-field stress, and therefore both contributions must be carefully evaluated, preferably in real-time, during drilling operations [9]. The need for real-time analysis is also the reason why superposed analytical solutions are still in vogue and cannot easily be replaced by solution methods that require gridding and have consequent longer computation times.

An additional concern is whether the standard plane stress solution of Kirsch [1] is accurate enough, whether a plane strain approach should be used, or any other approach. The plane stress solution is an end member solution for so-called thin plates; the other end member would be a thick-plate approach (plane strain assumption); each is often portrayed as 2D solution but in fact considers the state of 3D strain and stress, respectively, at all times. Although prior studies have evaluated the difference between plane strain and plane stress solutions, typically only the maximum stress concentrations are compared without analyzing the stress states further away from the boreholes. Also, the effect of the internal pressure loading superposed in the far-field stress anisotropy is normally only evaluated for arbitrarily chosen cases, which is why additional systematic evaluations in our study are merited.

Other concerns arise when multiple wells are drilled in close proximity from the same surface location and the stress interference due to the mutual interaction between the wells needs to be accounted for in the wellbore stability models. Our analysis considers both single-hole solutions and solutions for the superposition of multi-holes, all with or without individually varying pressure loads in addition to the far-field stress loading. The method of solution used is the linear superposition method (LSM) first named in ref. [3], which adds the elastic displacement vectors due to various contributions (usually boundary forces) to the elastic distortion and then solves the stress tensor field using an appropriate constitutive equation for linear elasticity.

The present analysis revisits the basic solutions for plane stress and plane strain, points out some earlier errors in displacement equations appearing in standard

textbooks, and then proceeds to compute and compare the two end-member solutions (plane stress and plane strain). We also quantify the delta between thin and thick-plate solutions for multi-hole problems using the LSM method (analytical superposition of displacements) for which plane stress solutions were first given in ref. [3]. Plane strain solutions are developed in the present study to quantify the delta between the solutions due to the assumed boundary condition. Additionally, the LSM multi-hole results are validated against—(1) photo-elastic contour patterns for a 5-hole problem of Kosłowska [10], and (2) a numerical example of Yi et al. [11]. The present study is limited to hole analysis based on a linear elasticity assumption for isotropic elastic plates; borehole analysis of anisotropic media was given in prior work [4, 9], applying equations developed for plane stress cases in [12].

2. Prior work

The petroleum, mining, and geotechnical tunneling industry have embraced the Kirsch equations for stability analysis of cylindrical boreholes in isotropic media. The governing equations for the Kirsch solution are based on Airy's stress function. A fact easily overlooked and little emphasized is that the equations introduced by Kirsch [1] assume a boundary condition of plane deviatoric stress, which would strictly limit the use of the Kirsch equations to cases that comply with the original boundary condition of plane stress. In spite of this limitation, the Kirsch equations are routinely applied in wellbore stability computations that may potentially yield inaccurate results if initially assumed boundary conditions in the analytical solutions are not met in the field application. For example, one may suggest that it may be more appropriate for deep boreholes in thick formations to use a thick-plate analysis (plane strain boundary condition), rather than the thin-plate analysis that fully justifies the use of the original Kirsch equations.

In nature and in real manufactured materials, the plane stress solution would only be valid for very large holes in very thin plates, such as for rivets in thin airfoils used in aircraft. However, for very thick elastic media perforated by tiny holes, such as in the case of boreholes penetrating rock formations of several kilometers thickness, the plane strain boundary condition seems more appropriate. We, therefore, evaluated what may be the actual inaccuracy creeping into the analysis of the stress concentration magnitude due to variations in the boundary conditions. Unwarranted wellbore stability problems may occur if the stress state in the well appears to deviate from plane stress proxy solutions. The delta between the stress solutions for the thin and thick-plate approaches is fully quantified in the present study for a variety of cases.

2.1 Evaluation by Clark

The notion that considerable differences may arise between stress magnitudes in elastic plates due to different transverse boundary conditions (such as plane stress versus plane strain) if subjected to otherwise the same far-field stress has been long recognized. That the stress differential may become significant was quantified in a study by Clark [13] for a uniform plate of finite, uniform thickness (and no holes) loaded with time-dependent far-field sinusoidal stresses at a lateral edge of the plate. Three cases were highlighted in ref. [13], scaling the problem with a typical wavelength, l , of the sinusoidal load and the plate thickness, $2h$. For $\frac{2h}{l} \rightarrow 0$, we have plane

stress (when the wavelength of stress applied is very large as compared to thickness). For $\frac{2h}{l} \rightarrow \infty$, we have plane strain (when the wavelength of stress applied is very small as compared to thickness). When the wavelength is comparable to the thickness $\frac{2h}{l} = 1$, the maximum stress at the edges of the plate may be up to 20% larger than for “elementary plane stress” (also termed “generalized plane stress” or “very thin plate theory”), which occurs when ($\frac{2h}{l} \rightarrow 0$). The stress concentration values obtained for $\frac{2h}{l} = 1$ exceed the plane strain solution ($\frac{2h}{l} \rightarrow \infty$) by 31%. Clark [13] also emphasized that the generalized 2D plane stress solution for isotropic elastic plates is independent of the Poisson’s ratio and neglects totally the transverse and normal stresses. Given the results of Clark [13], it is by no means obvious whether we may neglect the variations in both the stress concentrations and the stress transverse to an elastic plate with finite thickness and a boundary condition that is somewhere close to halfway between plane strain and plane stress. Below we discuss this quandary of the impact of boundary conditions on stress concentrations and transverse stresses for isotropic elastic plates with circular holes. Although the stress magnitude differentials according to ref. [13] may not be applicable to static loading cases (see later), borehole stability may be adversely impacted by seismic events, given the considerable differences in stress magnitude solutions when sinusoidal stress loads of different wavelengths are applied.

2.2 Evaluation by Green

Green [14] considered a linear elastic plate scaled by thickness $2h$ perforated by a hole of typical radius a . He introduced a practical dimensionless scaling parameter $\frac{a}{h}$ with hole radius in the nominator and plate half-thickness in the denominator. For a thick plate ($\frac{a}{h} \rightarrow 0$), a plane strain boundary condition can be assumed (in this case the strain in the z -direction $\varepsilon_{zz} = 0$). For a thin-plate solution ($\frac{a}{h} \rightarrow \infty$), a plane stress boundary condition can be assumed (in this case the stress in the z -direction $\sigma_{zz} = 0$). The impact of boundary conditions—on the stress concentrations and transverse stresses in elastic plates with circular holes—that are midway between those leading to either perfect plane stress or perfect plane strain cases were reviewed by Green [14]. He posited that the case $\frac{a}{h} = 1$ would lie midway between the two extremes of plane strain ($\frac{a}{h} \rightarrow 0$) and plane stress ($\frac{a}{h} \rightarrow \infty$) boundary conditions. Based on 3D calculations for the case $\frac{a}{h} = 1$ (“midway” boundary condition), the stress concentration halfway the total depth of the plate at $z = 0$ in the rim of a single hole in a location transverse to the applied far-field stress, $\sigma_{xx-\infty}$, increased to $3.10 \sigma_{xx-\infty}$. If $\sigma_{xx-\infty} > 0$, we have a tension under the engineering sign convention, and hence $3.10 \sigma_{xx-\infty}$ is an increased tension. At the plate’s surface $z = h$ (for the case $\frac{a}{h} = 1$), the maximum stress concentration was less: $2.81 \sigma_{xx-\infty}$.

For both plane strain and generalized plane stress, the maximum stress concentration averaged over the thickness of the plate should be equal to $3\sigma_{xx-\infty}$ [14]. This solution is exact for plane strain (thick plates) where—from a theoretical point of view—there may exist no variation in the maximum stress concentration near the hole for any depth z . However, for the finite-thickness plate (case with $\frac{a}{h} = 1$), only the averaged value will be $3\sigma_{xx-\infty}$, as is evident from [14] treatise. Again, at $z = 0$ at the rim of a single hole, we have $3.10 \sigma_{xx-\infty}$ (+3% different from $3\sigma_{xx-\infty}$), while at the surface of the plate at $z = h$, the maximum stress concentration was lowered to $2.81\sigma_{xx-\infty}$ (−6% different from $3 \sigma_{xx-\infty}$). The stress attenuation at the hole rim in the

longitudinal direction parallel to $\sigma_{xx-\infty}$ appeared to vary from $-1.10 \sigma_{xx-\infty}$ at $z = 0$ (a compression +10% above $-\sigma_{xx-\infty}$), while at the surface of the plate at $z = h$ the stress concentration was $-0.81 \sigma_{xx-\infty}$ (19% below $-\sigma_{xx-\infty}$). Likewise, in ref. [15], Yang et al. found stress concentrations between two interacting holes in a finite-thickness elastic plate are maximum only at $z = 0$, but decrease toward the surface of the plate ($z \rightarrow h$). Also, as the plates thicken, the maximum stress concentration shifts gradually to the surface of the plates.

According to [16] “generalized plane stress”-theorem, variations in stress concentration values throughout the thickness of a plate coinciding with the (x, y) -plane can be neglected and only the average values of the remaining stress are estimated. However, as Green [14] showed for solutions at the rim of a circular hole, there will be variations in stress concentrations over depth $0 \leq z \leq h$ when the plate has a finite thickness, characterized by $\frac{a}{h}$. However, for $\frac{a}{h} = 1$, the average maximum stress concentration would only deviate about 3% from the average values. Green [14] concluded that the generalized plane stress theory gives “fairly good” estimations for the average values of stress concentrations at the hole in a stressed plate with boundary conditions “midway” between plane stress and plane strain (adopting $\frac{a}{h} = 1$ for this case).

2.3 Other evaluations

In our opinion, there can be little doubt that plane strain is the obvious boundary condition when boreholes are drilled in thick formations. So, the question is, what (if any) corrections are necessary when applying the Kirsch equations for plane stress to compute the stress concentrations near real-world boreholes. This question is addressed below considering two cases (A and B), as previously evaluated in ref. [4].

The plane stress boundary condition ($\sigma_{zz} = \sigma_{xz} = \sigma_{yz} = 0$) assumed in the Kirsch solution in ref. [1] implies that the mean stress $\bar{\sigma}$ in the thin elastic plate ($\frac{a}{h} \rightarrow \infty$) is everywhere given by: $\bar{\sigma} = \frac{\sigma_{xx} + \sigma_{yy}}{3}$ (Case A). For plane strain, the mean stress $\bar{\sigma}^*$ within the thick plate’s (x, y) -plane of the thick plate ($\frac{a}{h} \rightarrow 0$) is given by $\bar{\sigma}^* = \frac{(1+\nu)(\sigma_{xx}^* + \sigma_{yy}^*)}{3}$ (Case B), introducing the Poisson’s ratio ν . The longitudinal stress is given by $\sigma_{zz}^* = \nu(\sigma_{xx}^* + \sigma_{yy}^*)$; the longitudinal strain along the borehole is absent $\epsilon_{zz}^* = 0$. For the special case of $\nu = 0$, the longitudinal stress will vanish, but rocks have Poisson’s ratio closer to 0.25.

We may assume that the mean stresses for adjacent plane strain and plane stress sections of a borehole will be nearly identical stress concentration requirements such that we may equate the mean stress expressions for Case A and for Case B, from which it follows that $\frac{\sigma_{xx} + \sigma_{yy}}{\sigma_{xx}^* + \sigma_{yy}^*} = 1 + \nu$. This relationship says that the magnitude of the principal stresses $\sigma_{xx} + \sigma_{yy}$ acting in a plane stress section of the borehole will be larger than the plane strain case $\sigma_{xx}^* + \sigma_{yy}^*$ by a factor $1 + \nu$ (about 125% in practice, using $\nu = 0.25$). For plane stress, the longitudinal strain component is given by $\epsilon_{zz} = -\frac{\nu}{E}(\sigma_{xx} + \sigma_{yy})$, where E is Young’s modulus of the material, which for practical situations with thin-bedded rock strata are negligibly small strains that can be easily accommodated by the discontinuities in strain occurring due to variations in the elastic constants when the drill bit moves from one rock layer into the next.

3. Methodology

The series of analytical expressions used to produce the solutions in Section 4 are outlined in Section 3. We start out with the generic elastic displacement equations for a single hole in an infinite plate subjected to far-field stress (Section 3.1), which can be solved for plane strain (Section 3.2) or plane stress (Section 3.3) boundary conditions. Although these expressions are basic, some confusing errors occur in both primary (journal papers) and secondary (textbooks) literature, which need to be pointed out (see respective sections below). What is new in our approach is that we do not solely focus on the stress concentrations at the hole but solve the stress magnitudes and principal stress orientations throughout the plates for a finite domain near the hole (Section 4) based on the equations given in Section 3.

The difference or delta between the stress magnitudes due to a plane strain or plane stress assumption is quantified in an explicit expression (Section 3.4). Because boreholes are commonly pressured from the inside by a net mud pressure, we also evaluate the displacements due to the internal pressure on the wellbore (Section 3.5). The equations of Sections 3.1–3.5 are all given in polar coordinates, but the far-field stresses in nature are typically uniform in Cartesian directions, which is why we switch to Cartesian coordinates in Sections 3.6. The use of Cartesian coordinates is essential for our analysis of both single-hole problems (Section 4.1) and multi-hole solutions (Section 4.2). Ultimately, when all the vector displacements have been computed and converted to strains, constitutive equations are needed (Section 3.7) to convert certain strain tensor fields, for any given set of elastic moduli to the corresponding stress field. The systematic series of equations in Sections 3.1 to 3.7 was used to produce the results in Section 4.

3.1 Hole displacement equations

In the theory of linear elasticity, stress quantities are linear functions of the displacement gradients expressed as strain quantities. Let us analyze the elastic displacements around a circular cylindrical hole of radius a , in an infinite plate subjected to far-field stress, $\sigma_{xx-\infty}$, acting along the x -axis. Analytical solutions for the displacement equations in polar coordinates (r, θ) are (see ref. [17]):

$$u_r = \frac{\sigma_{xx-\infty}}{8G} a \left\{ \frac{r}{a} (\kappa - 1 + 2 \cos 2\theta) + \frac{2a}{r} \left[1 + \left(\kappa + 1 - \frac{a^2}{r^2} \right) \cos 2\theta \right] \right\} \quad (1)$$

$$u_\theta = \frac{\sigma_{xx-\infty}}{8G} a \left[-\frac{2r}{a} + \frac{2a}{r} \left(1 - \kappa - \frac{a^2}{r^2} \right) \right] \sin 2\theta \quad (2)$$

Above expressions capture the displacements for either plane strain or plane stress, depending upon the value inserted for κ , to be readily able to convert solutions for plane stress to plane strain, and vice-versa. In the above example, the solution for plane strain is given by substituting $\kappa = 3 - 4\nu$; for plane stress, one should use $\kappa = (3 - \nu)/(1 + \nu)$. Physically, the plane stress boundary condition applies to thin plates, while the plane strain condition applies to thick plates. The delta between the displacements and associated stress concentrations outcomes of the two approaches has not been made explicit, either for single or multiple holes, in any prior study.

3.2 Plane strain solution for the hole with uniaxial far-field stress

Using Eqs. (1) and (2) and substituting $\kappa = 3 - 4\nu$ for plane strain, the displacement solutions are:

$$u_r = \frac{\sigma_{xx-\infty}}{4Gr} \left\{ r^2(1 - 2\nu + \cos 2\theta) + a^2 \left[1 + \left(4(1 - \nu) - \frac{a^2}{r^2} \right) \cos 2\theta \right] \right\} \quad (3)$$

$$u_\theta = -\frac{\sigma_{xx-\infty}}{4Gr} \left[r^2 + a^2 \left(2(1 - 2\nu) + \frac{a^2}{r^2} \right) \right] \sin 2\theta \quad (4)$$

The above expressions for plane strain may be formulated using Young's modulus, E , instead of the shear modulus, G , substituting $G = E/2(1 + \nu)$ into Eqs. (3) and (4):

$$u_r = \sigma_{xx-\infty} \left(\frac{1 + \nu}{2Er} \right) \left\{ r^2(1 - 2\nu + \cos 2\theta) + a^2 \left[1 + \left(4(1 - \nu) - \frac{a^2}{r^2} \right) \cos 2\theta \right] \right\} \quad (5)$$

$$u_\theta = -\sigma_{xx-\infty} \left(\frac{1 + \nu}{2Er} \right) \left[r^2 + a^2 \left(2(1 - 2\nu) + \frac{a^2}{r^2} \right) \right] \sin 2\theta \quad (6)$$

It is worth noting that a textbook by Goodman [18] has wrongly truncated terms in his Eq. (7.2a) and a sign error occurs in his Eq. (7.2b). Moreover, Kirsch's Equations [1] are quoted in his Eq. (7.1a-c) with a wrong statement that these would be valid for plane strain; the quoted equations are for plane stress boundary conditions. Several other sources [19-20] have promulgated the use of wrong equations similar to Goodman's (without mentioning the source). The original Kirsch equations are widely used, but also widely misused or marred by misprinted equations in the literature. For example, Eq. (3.15) in [21] has a typo, and dropped a plus sign between two terms, for the radial stress around a single borehole.

3.3 Plane stress solution for the hole with uniaxial far-field stress

With the expressions of Sections 2.1 and 2.3 in place, we now solve Eqs. (1) and (2) for plane stress by substituting $\kappa = (3 - \nu)/(1 + \nu)$; the corresponding displacement solutions are:

$$u_r = \frac{\sigma_{xx-\infty}}{4Gr} \left\{ \frac{1 - \nu}{1 + \nu} r^2 + a^2 + \left(\frac{4a^2}{1 + \nu} + r^2 - \frac{a^4}{r^2} \right) \cos 2\theta \right\} \quad (7)$$

$$u_\theta = -\frac{\sigma_{xx-\infty}}{4Gr} \left[\frac{1 - \nu}{1 + \nu} 2a^2 + r^2 + \frac{a^4}{r^2} \right] \sin 2\theta \quad (8)$$

The above expressions for plane stress may be formulated using Young's modulus, E , instead of the shear modulus, G , substituting $G = E/2(1 + \nu)$ into Eqs. (7) and (8):

$$u_r = \sigma_{xx-\infty} \left(\frac{1 + \nu}{2Er} \right) \left\{ \frac{1 - \nu}{1 + \nu} r^2 + a^2 + \left(\frac{4a^2}{1 + \nu} + r^2 - \frac{a^4}{r^2} \right) \cos 2\theta \right\} \quad (9)$$

$$u_\theta = -\sigma_{xx-\infty} \left(\frac{1 + \nu}{2Er} \right) \left[\frac{1 - \nu}{1 + \nu} 2a^2 + r^2 + \frac{a^4}{r^2} \right] \sin 2\theta \quad (10)$$

Eqs. (9) and (10) are identical to those given in [22] (p. 740–742) and were used in a prior study focused on multi-hole problems under plane stress [3].

Separately, we checked for the computational integrity of the plane strain displacement solutions of Section 3.2 by applying a standard conversion substitution, as explained in Appendix A.

3.4 Delta between plane strain and plane stress solutions with uniaxial far-field stress

The residual displacements when subtracting Eqs. (9) from (5), and (10) from (6), respectively, are:

$$\begin{aligned}
 u_r &= \sigma_{xx-\infty} \left(\frac{1+\nu}{2Er} \right) \left\{ \left[r^2(1-2\nu + \cos 2\theta) + a^2 \left[1 + \left(4(1-\nu) - \frac{a^2}{r^2} \right) \cos 2\theta \right] \right] \right. \\
 &\quad \left. - \left[\frac{1-\nu}{1+\nu} r^2 + a^2 + \left(\frac{4a^2}{1+\nu} + r^2 - \frac{a^4}{r^2} \right) \cos 2\theta \right] \right\}, \\
 &= -\sigma_{xx-\infty} \left(\frac{\nu^2}{Er} \right) \{ r^2 + 2a^2 \cos 2\theta \}. \tag{11}
 \end{aligned}$$

$$\begin{aligned}
 u_\theta &= -\sigma_{xx-\infty} \left(\frac{1+\nu}{2Er} \right) \left\{ \left[r^2 + a^2 \left(2(1-2\nu) + \frac{a^2}{r^2} \right) \right] \sin 2\theta - \left(\frac{1-\nu}{1+\nu} 2a^2 + r^2 + \frac{a^4}{r^2} \right) \sin 2\theta \right\} \\
 &= \sigma_{xx-\infty} \left(\frac{\nu^2}{Er} \right) (2a^2 \sin 2\theta). \tag{12}
 \end{aligned}$$

3.5 Plane strain and plane stress solutions for the hole with internal pressure

From [23] general solution for a hollow cylinder (with infinite axial length) pressured inside and outside with different pressures, can be obtained a simple displacement solution for a hole in an infinite plate by letting the outer radius of the cylinder go to infinity such that only the term remains for the radial displacement due to the pressure inside the cylinder:

$$u_r = -P \frac{a^2}{r} \frac{1+\nu}{E} = -P \frac{a^2}{r} \frac{1}{G} \tag{13}$$

$$u_\theta = 0 \tag{14}$$

Above displacement field is due to a hole internally pressurized under plane strain boundary conditions and assumes P is given as a negative value when causing compression (as in mechanical engineering sign conventions); if we prefer to use P as a positive input, the minus sign in Eq. (13) must be dropped. Following ref. [3], we will consider positive P inputs (so minus sign will be dropped from Eq. (13) in the rest of this paper).

Plane strain solutions formulated with G can be converted to plane stress solutions by replacing ν with $\frac{\nu}{1+\nu}$ (e.g., [17], page 115). Eq. (13) when formulated with

G is identical to the plane strain solution, as applied in ref. [3], which means the plane stress solution is independent of ν . Therefore, the delta or residual displacement, in this case, will be zero. The displacement solution for an internally pressured hole in an infinite plate appears insensitive to the thickness of the plate, which can be understood via physical reasoning as follows. Adopting the definitions in [14] treatise on 3D stress systems in isotropic plates, for $\frac{a}{h} \rightarrow \infty$ we have a thin-plate problem (plane stress) and for $\frac{a}{h} \rightarrow 0$ we have a thick-plate problem (plane strain). In all 3D solutions for plane stress and plane strain cases, the solutions are identical in planes midway the plates at $h = 0$. However, when the plates possess a finite thickness, differences in solutions for plates with holes subjected to a far-field stress under plane strain and plane stress arise when studying solutions, where $h \rightarrow 0$. The internally pressured hole solution is insensitive to plate thickness, because for both plane strain and plane stress cases, the pressure on the hole is assumed uniform along h , so essentially does not allow stresses to occur normal to the plate by strictly maintaining the pressure equal to P even at the rim of the hole near the surface (see Section 4).

3.6 Conversion to Cartesian coordinates

The conversion of the displacement solutions from polar to Cartesian coordinates is practical for single-hole and multi-hole analysis (which requires superposition) of practical borehole problems because the far-field (tectonic) stresses are assumed more or less constant in the three individual Cartesian directions. It is emphasized here that the solutions in Cartesian and polar coordinates only differ in coordinate transformation to facilitate the visualization of either polar or Cartesian vector displacements, each with their corresponding solutions for the stress and strain tensor components. However, the principal stresses remain invariant to the coordinate system used. The conversion from polar to Cartesian coordinates follows the same steps as in Eqs. (12–17) of ref. [3].

3.6.1 Cartesian coordinates of plane strain solutions (uniaxial far-field stress)

The displacement Eqs. (5) and (6) in polar vector coordinates (u_r, u_θ) are converted to Cartesian displacements vector coordinates (u_x, u_y) using the appropriate coordinate transformation equations (see Appendix B for details):

$$u_x = u_r \cos \theta - u_\theta \sin \theta, \quad u_y = u_r \sin \theta + u_\theta \cos \theta$$

We get:

$$u_x = \sigma_{xx-\infty} \left(\frac{1+\nu}{2E} \right) \left\{ \left[(x^2+y^2)(1-2\nu) + x^2 - y^2 + a^2 + 4a^2(1-\nu) \left(\frac{x^2-y^2}{x^2+y^2} \right) - a^4 \left(\frac{x^2-y^2}{(x^2+y^2)^2} \right) \right] \left(\frac{x}{x^2+y^2} \right) + \left[2xy + (1-2\nu) \left(\frac{4a^2xy}{x^2+y^2} \right) + \frac{2a^4xy}{(x^2+y^2)^2} \right] \left(\frac{y}{x^2+y^2} \right) \right\} \quad (15)$$

$$u_y = \sigma_{xx-\infty} \left(\frac{1+v}{2E} \right) \left\{ \left[(x^2 + y^2)(1-2\nu) + x^2 - y^2 + a^2 + 4a^2(1-\nu) \left(\frac{x^2 - y^2}{x^2 + y^2} \right) - a^4 \left(\frac{x^2 - y^2}{(x^2 + y^2)^2} \right) \right] \left(\frac{y}{x^2 + y^2} \right) - \left[2xy + (1-2\nu) \left(\frac{4a^2xy}{x^2 + y^2} \right) + \frac{2a^4xy}{(x^2 + y^2)^2} \right] \left(\frac{x}{x^2 + y^2} \right) \right\} \quad (16)$$

3.6.2 Cartesian coordinates of plane stress solutions (uniaxial far-field stress)

The displacement Eqs. (9) and (10) were converted to Cartesian coordinate in ref. [3] as:

$$u_x = \sigma_{xx-\infty} \left(\frac{1+v}{2E} \right) \left\{ \left[\frac{1-\nu}{1+\nu} (x^2 + y^2) + a^2 + \left(\frac{4a^2}{1+\nu} + x^2 + y^2 - \frac{a^4}{x^2 + y^2} \right) \left(\frac{x^2 - y^2}{x^2 + y^2} \right) \right] \times \left(\frac{x}{x^2 + y^2} \right) + \left[\left(\frac{1-\nu}{1+\nu} 2a^2 + x^2 + y^2 + \frac{a^4}{x^2 + y^2} \right) \left(\frac{2xy}{x^2 + y^2} \right) \right] \left(\frac{y}{x^2 + y^2} \right) \right\} \quad (17)$$

$$u_y = \sigma_{xx-\infty} \left(\frac{1+v}{2E} \right) \left\{ \left[\frac{1-\nu}{1+\nu} (x^2 + y^2) + a^2 + \left(\frac{4a^2}{1+\nu} + x^2 + y^2 - \frac{a^4}{x^2 + y^2} \right) \left(\frac{x^2 - y^2}{x^2 + y^2} \right) \right] \times \left(\frac{y}{x^2 + y^2} \right) - \left[\left(\frac{1-\nu}{1+\nu} 2a^2 + x^2 + y^2 + \frac{a^4}{x^2 + y^2} \right) \left(\frac{2xy}{x^2 + y^2} \right) \right] \left(\frac{x}{x^2 + y^2} \right) \right\} \quad (18)$$

Eqs. (15)–(18) are valid for a borehole centered at the origin. For holes with their centers shifted to an arbitrary location (x_s, y_s) , we replace x by $(x - x_s)$ and y by $(y - y_s)$. For multiple wellbore problems, as in ref. [3], we add the following terms to Eqs. (15) and (16) for the plane strain case:

$$u_x = \frac{-(n-1)}{n} \frac{\sigma_{xx-\infty}(1-\nu^2)}{E} x \quad (19)$$

$$u_y = \frac{(n-1)}{n} \frac{\sigma_{xx-\infty}\nu(1-\nu^2)}{E(1-\nu)} y \quad (20)$$

and the following terms to Eqs. (17) and (18) for the plane stress case:

$$u_x = \frac{-(n-1)}{n} \frac{\sigma_{xx-\infty}}{E} x \quad (21)$$

$$u_y = \frac{(n-1)}{n} \frac{\sigma_{xx-\infty}\nu}{E} y \quad (22)$$

where n denotes the number of boreholes. The total displacement vectors ($u_{x,\text{total}}$ and $u_{y,\text{total}}$) due to all holes combined can be computed by the following summations:

$$u_{x,\text{total}} = \sum_{i=1}^n u_{x,i} \quad (23)$$

$$u_{y,\text{total}} = \sum_{i=1}^n u_{y,i} \quad (24)$$

3.6.3 Cartesian coordinates of delta between plane strain and plane stress solutions (uniaxial far-field stress)

Using the same transformation as in Section 3.6.1, Eqs. (11) and (12) are converted to Cartesian coordinate (see Appendix B for details):

$$u_x = -\sigma_{xx-\infty} \left(\frac{v^2}{E(x^2 + y^2)} \right) \left[\left(x^2 + y^2 + 2a^2 \frac{x^2 - y^2}{x^2 + y^2} \right) x + \left(4a^2 \frac{xy}{x^2 + y^2} \right) y \right] \quad (25)$$

$$u_y = -\sigma_{xx-\infty} \left(\frac{v^2}{E(x^2 + y^2)} \right) \left[\left(x^2 + y^2 + 2a^2 \frac{x^2 - y^2}{x^2 + y^2} \right) y - \left(4a^2 \frac{xy}{x^2 + y^2} \right) x \right] \quad (26)$$

One can also obtain Eqs. (25) and (26) by subtracting Eqs. (17) and (18) from Eqs. (15) and (16) (see Appendix B).

3.6.4 Cartesian coordinates of plane stress/plane strain solutions for a single hole with internal pressure

The polar coordinate solutions of Section 3.5 have been transformed to Cartesian coordinates, using the appropriate coordinate transition equations of Section 3.6.1:

$$u_x = P \left(\frac{a^2}{x^2 + y^2} \right) \left(\frac{1 + \nu}{E} \right) x \quad (27)$$

$$u_y = P \left(\frac{a^2}{x^2 + y^2} \right) \left(\frac{1 + \nu}{E} \right) y \quad (28)$$

3.7 Constitutive equations

From the displacement field equations, once converted to Cartesian coordinates, one may compute the displacement gradients to obtain the strain tensor components in every location of the elastic medium:

$$\varepsilon_{xx} = \frac{\partial u_x}{\partial x} \quad (29)$$

$$\varepsilon_{yy} = \frac{\partial u_y}{\partial y} \quad (30)$$

$$\varepsilon_{xy} = \frac{1}{2} \left[\frac{\partial u_x}{\partial y} + \frac{\partial u_y}{\partial x} \right] \quad (31)$$

In the present study, we follow the mechanical engineering convention where extension and tension are positive. Once the strain components have been identified for our specific problem, the stresses in each point of the elastic medium can be resolved using the constitutive equations. The following equations are valid for either plane strain or plane stress, depending on the value assigned to κ with a linear elasticity assumption [17]:

$$\varepsilon_{xx} = \frac{1}{8G} [(\kappa + 1)\sigma_{xx} + (\kappa - 3)\sigma_{yy}] \quad (32)$$

$$\varepsilon_{yy} = \frac{1}{8G} [(\kappa - 3)\sigma_{xx} + (\kappa + 1)\sigma_{yy}] \quad (33)$$

$$\varepsilon_{xy} = \frac{\sigma_{xy}}{2G} \quad (34)$$

The constitutive equation for plane strain is given by substituting $\kappa = 3 - 4\nu$; for plane stress, one should use $\kappa = (3 - \nu)/(1 + \nu)$. Separately, when G is used in the equations, the solutions for plane stress may be converted to plane strain by replacing ν with $\nu/(1 - \nu)$, which means replacing $(3 - \nu)/(1 + \nu)$ by $(3 - 4\nu)$. Likewise, solutions for plane strain may be converted to plane stress by replacing ν with $\nu/(1 + \nu)$, which means replacing $(3 - 4\nu)$ by $(3 - \nu)/(1 + \nu)$. The strain in the z -direction, ε_{zz} , vanishes for plane strain but does not necessarily vanish for plane stress ($\sigma_{zz} = \sigma_{xz} = \sigma_{yz} = 0$) where it is given by:

$$\varepsilon_{zz} = -\frac{\nu}{E} (\sigma_{xx} + \sigma_{yy}) = -\frac{\nu}{1 - \nu} (\varepsilon_{xx} + \varepsilon_{yy}) \quad (35)$$

The principal strain magnitude can now be obtained as follows:

$$\varepsilon_1, \varepsilon_2 = \frac{\varepsilon_{xx} + \varepsilon_{yy}}{2} \pm \sqrt{\left(\frac{\varepsilon_{xx} - \varepsilon_{yy}}{2}\right)^2 + \varepsilon_{xy}^2} \quad (36)$$

4. Results

A MATLAB code was written to evaluate—for specific hole arrangements—the delta between the plane strain and the plane stress solutions based on the algorithms developed in Section 3. We consider holes of equal and different radii, with and without far-field stress, with and without internal pressures, and the pressure of individual holes may be varied. All solutions given are for static conditions, in the sense that time-dependent changes are not considered in the present study. Two types of borehole problems are addressed: single hole (Section 4.1) and multi-hole (Section 4.2).

4.1 Single-hole problems

The principal stress distributions σ_1 and σ_2 are computed using

$$\sigma_1 = \frac{1}{2} (\sigma_{xx} + \sigma_{yy}) + \left[\sigma_{xy}^2 + \frac{1}{4} (\sigma_{xx} - \sigma_{yy})^2 \right]^{\frac{1}{2}} \quad (37)$$

$$\sigma_2 = \frac{1}{2} (\sigma_{xx} + \sigma_{yy}) - \left[\sigma_{xy}^2 + \frac{1}{4} (\sigma_{xx} - \sigma_{yy})^2 \right]^{\frac{1}{2}} \quad (38)$$

Inputs	
Hole positions (x, y)	(0,0)
Hole radii, a [m]	0.2
Poisson's ratio, ν [-]	0.3
Far-field stress, σ [MPa]	10
Internal pressure, P [MPa]	10
Number of boreholes, n	1
Young's modulus, E [GPa]	50

Table 1.
 Model inputs used for the single-hole problem.

The first case considers a single hole subject to either.

Case 1-1: a far-field stress only,

Case 1-2: an internal pressure only,

Case 1-3: the superposed Cases 1-1 and 1-2.

Model inputs are given in **Table 1**. A comprehensive comparison of the vector displacement fields, strain tensor components, principal strains, stress tensor components, and principal stresses for all the above cases is given in Appendix C.

4.1.1 Case 1-1: single hole subject to a far-field stress

Figure 1 quantifies the delta of the principal stress distributions σ_1 and σ_2 for the plane strain and plane stress boundary conditions in the case of applying far-field

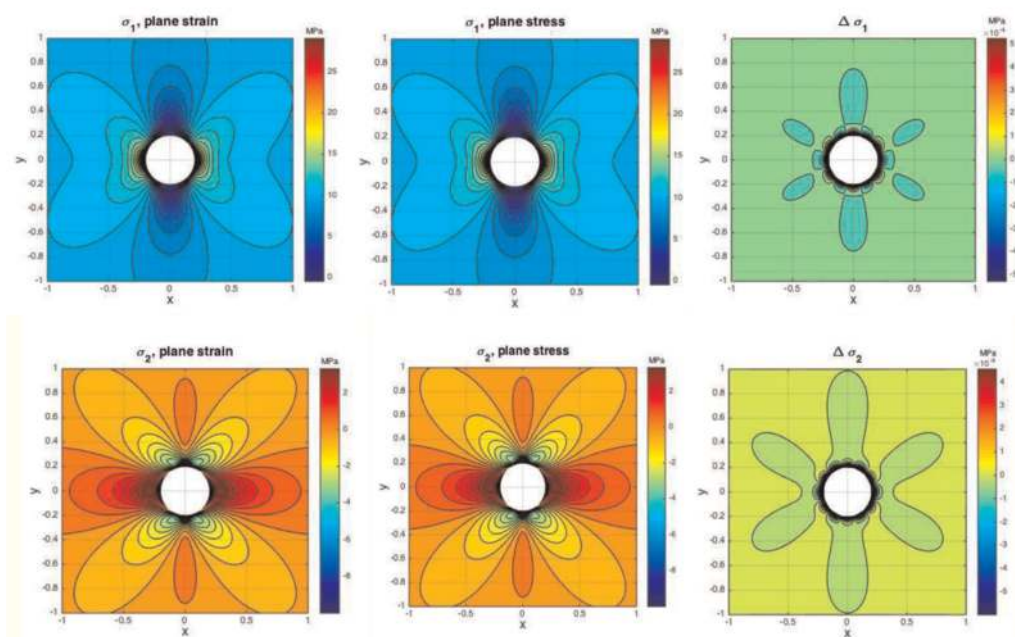


Figure 1.
 Principle stress distributions σ_1 (top row) and σ_2 (bottom row) for single hole subject to far-field stress. The first column is for plane strain boundary conditions, the second column is for plane stress boundary conditions, and the third column quantifies the difference (delta) between the first and second cases.

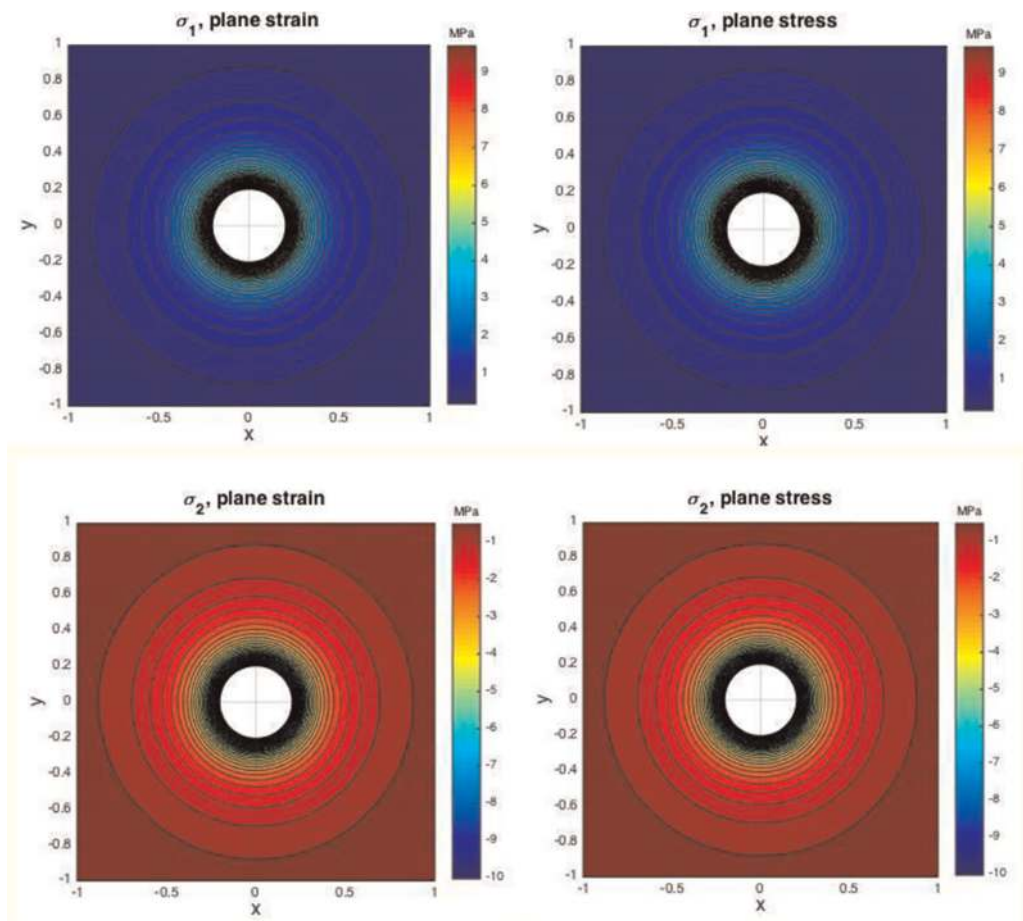


Figure 2. Principle stress distributions σ_1 (top row) and σ_2 (bottom row) for single hole subject to internal pressure. The first column is for the plane strain boundary condition; the second column is for the plane stress boundary condition.

stress only. The first column in **Figure 1** is for plane strain boundary conditions, the second column is for plane stress boundary conditions, and the third column represents the residual of the principal stress magnitude.

4.1.2 Case 1-2: single hole subject to internal pressure

For the hole using only internal pressure, the principal stress solutions for plane strain and plane stress are identical (**Figure 2**) due to the same displacement fields (see the reasoning in Section 3.5).

4.1.3 Case 1-3: superposed cases 1-1 and 1-2

The superposed Cases 1-1 and 1-2 seem trivial, but the deltas in **Figure 3** differ from those in **Figure 1**. The explanation is that the displacements due to the internal pressure on the hole add lateral uniform volumetric displacements that shift the locations where the deltas occur. When the internal pressure on the hole increases, the overall delta remains limited.

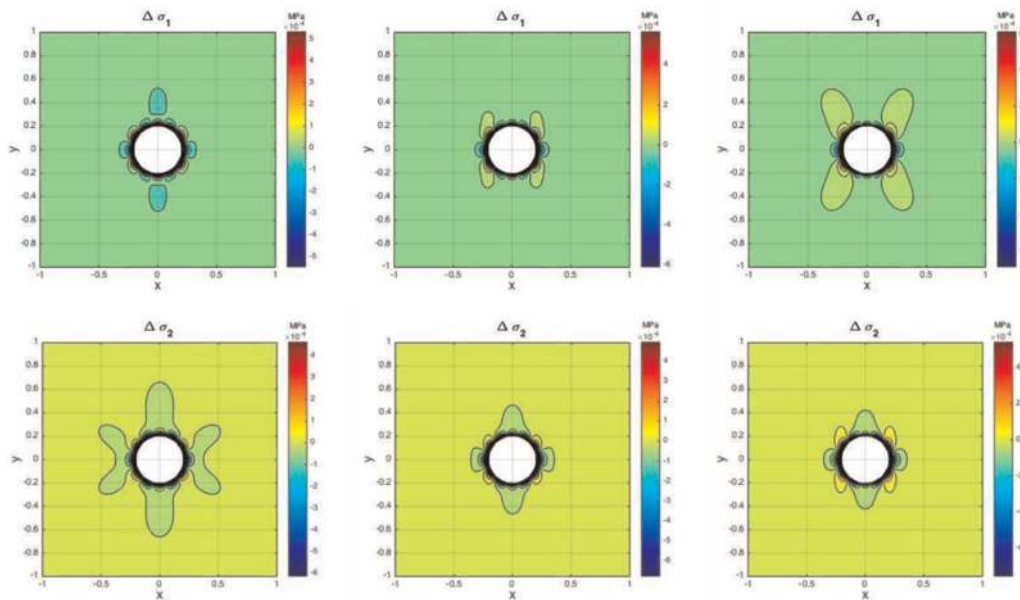


Figure 3.
The residual of the principle stress distributions σ_1 (top row) and σ_2 (bottom row) for a single hole subject to far-field stress (10 MPa) and different internal pressure loads (first column: $P = 1$ MPa, second column: $P = 5$ MPa, and third column: $P = 10$ MPa).

4.2 Multi-hole problems

For multi-hole modeling, the elastic displacements due to the individual contributions are superposed, then converted to the overall stress state via the constitutive equations. The procedure has been previously applied and was coined the Linear Superposition Method (LSM) in prior work. For perfect analytical accuracy of LSM multi-hole solutions, the superposition patterns would require perfect symmetry patterns for hole arrangements and endless repetitions as in the method of images. This symmetrical superposition principle also lies at the heart of earlier analytical multi-hole stress interference solutions [24–27].

A previous multi-hole solution departing from symmetric superposition by instead using randomly placed holes was assumed a valid approach [28]. The 11-hole problem in ref. [28], solved by them with a system of linear algebraic equations using a complex boundary integral method based on truncated Fourier series, was closely matched with an LSM solution [29]. We are well aware that LSM solutions for arbitrarily placed holes would be only asymptotically correct, due to hole patterns lacking symmetry. However, based on close matches of LSM-based solutions with photo-elastic patterns in our prior studies [4], as well as a comparison against Abaqus solutions in [30] our conclusion was that LSM gives very reliable results even for randomly placed hole arrangements.

To further support the practical reliability of LSM solutions for randomly placed holes, several new comparisons of stress field solutions with LSM for multi-hole problems with those obtained with other methods are given below. These comparisons are for a photo-elastic prototype strain and stress visualization (Case 2–1) and a prototype solution based on a finite element solution method (Case 2–2).

4.2.1 Case 2–1: photo-elastic prototype

For multi-hole analysis, we first consider a traditional example of photo-elastic visualization of displacement and strain components. The 5-hole photo-elastic prototype (**Figure 4**) has a total thickness of 5 mm (3 mm aluminum and 2 mm photo-elastic coating). The aluminum strips are 100 mm wide and 450 mm long. The long dimension may be assumed well suited for an infinite plate solution. However, the lateral width of 100 mm leaves only 30 mm between the boundaries of the outer holes (all have radii of 10 mm) and the left and right boundaries of the elastic plate.

A point that has been little elaborated is whether photo-elastic experiments typically represent thin- or thick-plate solutions, that is, represent plane stress or plane strain solutions. Theoretically, solutions for a plane stress boundary condition would apply to holes in very thin strips (for which σ_{zz} will be negligibly small). However, when a plate is “thicker” instead of $\sigma_{zz} \rightarrow 0$, we will have the $\epsilon_{zz} \rightarrow 0$, and the boundary condition approaches a plane strain case. For exactly what “finite thickness” of an elastic strip with holes, the plane stress solutions would need to be replaced by a plane strain solution has never been made explicit.

The accurate LSM solutions for either an infinite plate [with thin plate ($\frac{a}{h} \rightarrow \infty$) or a thick plate ($\frac{a}{h} \rightarrow 0$) solutions] will not be able to perfectly match the photo-elastic prototype with finite width, finite length, and for $0 < \frac{a}{h} < \infty$. Nonetheless, we can still use LSM to investigate which solution (plane strain or plane stress) gives the best approximation for a particular case. We tested for both, following [14] reasoning (summarized in Section 2.2 of the present study), for $\frac{a}{h} \rightarrow \infty$ we have a thin-plate problem (plane stress); for $\frac{a}{h} \rightarrow 0$ we have a thick-plate problem (plane strain).

4.2.2 Case 2–1: results

Model inputs are given in **Table 2**. Match attempts of **Figure 4 b-d** contour patterns with plane strain and plane stress LSM codes are given in **Figures 5–7**,

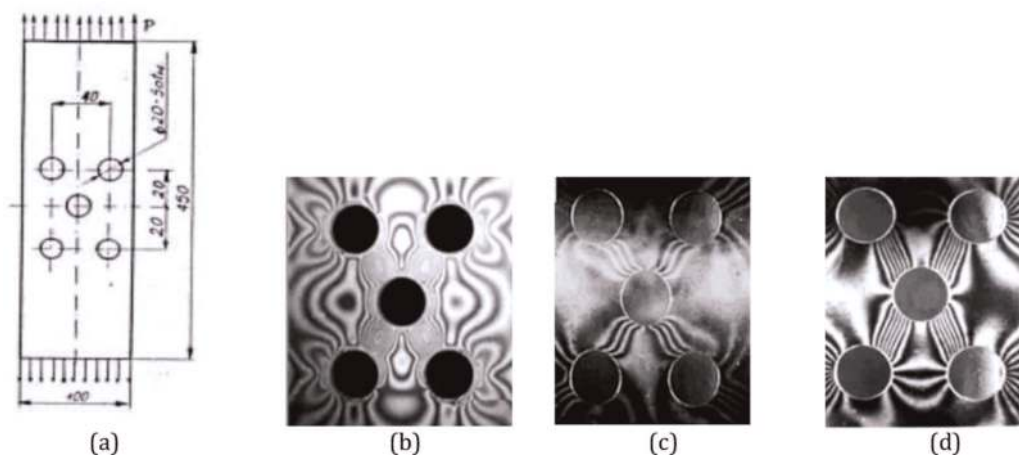


Figure 4. The 5-hole photo-elastic prototype. (a) Plate dimensions, (b) isochromatic pattern for strain state, (c) $u(x,y)$ displacement magnitude contours, (d) $v(x,y)$ displacement magnitude contours (after [10]).

Inputs		
hole positions (x, y)	Center hole	(0,0)
	Top right	(0.3,0.2)
	Top left	(-0.3,0.2)
	Bottom left	(-0.3,-0.2)
	Bottom right	(0.3,-0.2)
Hole radii, a [m]		0.1
Poisson's ratio, ν [-]		0.4
Far-field stress, σ [MPa]		10
Number of boreholes, n		5
Young's modulus, E [GPa]		50

Table 2.
 Model inputs used for 5-hole problem.

respectively. Any mismatches near the right and left margins of the sample may be due to differences in lateral boundary conditions: the photo-elastic strip has a finite width, while our solutions are for an infinite plate. The lateral boundary may be simulated by a mirror-image approach, but was not pursued in the present study. Separately, comprehensive comparisons of the vector displacement fields, strain tensor components, principal strains, stress tensor components, and principal stresses are given in Appendix D.

For the elastic prototype of **Figure 4**, the model scaling used was $\frac{a}{h} = 2$, which means the elastic displacement field (**Figures 6 and 7**) and resulting strain state (**Figure 5**) in the plane of view represent the plane stress solution. The LSM method is used in this example for both plane stress and plane strain solution to validate this theoretical result. Clearly, the LSM plane stress solutions (**Figures 5c-7c**) are closer (but not “exactly”) to the contour patterns in **Figures 5a-7a**, respectively, than the LSM plane strain solutions (**Figures 5b-7b**).

4.2.3 Case 2-2: Numerical benchmark; solution paths

The accuracy of the LSM-based solutions was benchmarked in prior studies [3, 29], against results from independent solution methods (e.g., [28]), with excellent matches. Here we benchmark LSM in a multi-hole solution against the independent numerical solution for the tangential stress concentrations in the rim of a 5-hole problem by Yi et al. [11]. The 5-hole configuration studied is part of an infinite plate subject to a uniaxial far-field compression, with dimensions as shown in **Figure 8**. The numerical solution method (based on the finite element method) was validated by Yi et al. [11] against a prior analytical-numerical solution (based on a Laurent series method [31]).

The 5-hole problem of **Figure 8** has its holes positioned slightly different than those in **Figure 4**. We used the exact same 5-hole setup as in **Figure 8** to solve the tangential stresses with our LSM code. To quantify the radial and tangential stresses in a particular polar coordinate system (r, θ) , one may follow two different computational paths.

Path 1: Use $x = r \cos \theta$ and $y = r \sin \theta$ as inputs for the Cartesian displacement equations. For specific locations (r, θ) , such as at the rim of the central hole in

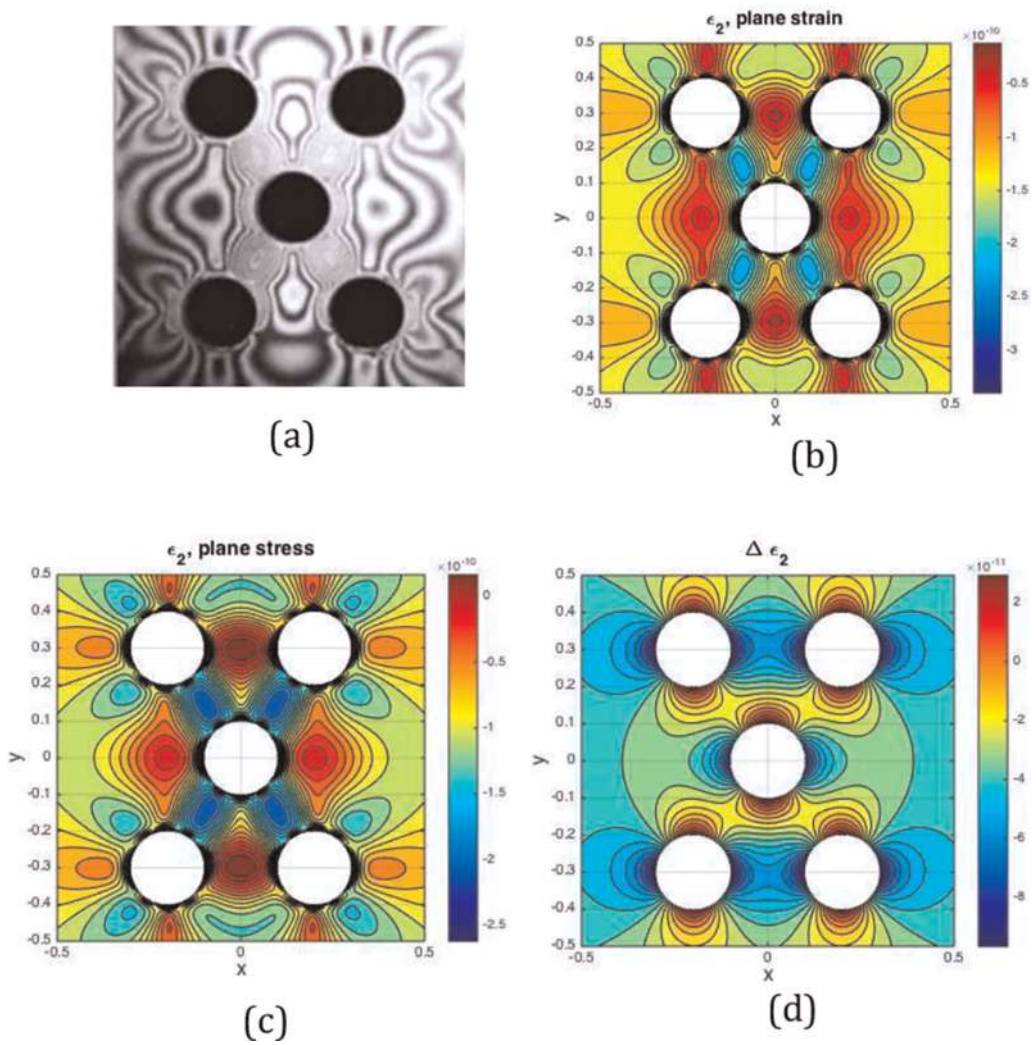


Figure 5. (a) Photo-elastic fringes near five equal holes due to far-field tension in the vertical direction of image view [10]. (b) LSM plane strain solution for ϵ_2 . (c) LSM plane stress solution for ϵ_2 . (d) the residual between the plane stress and plane strain solutions for ϵ_2 .

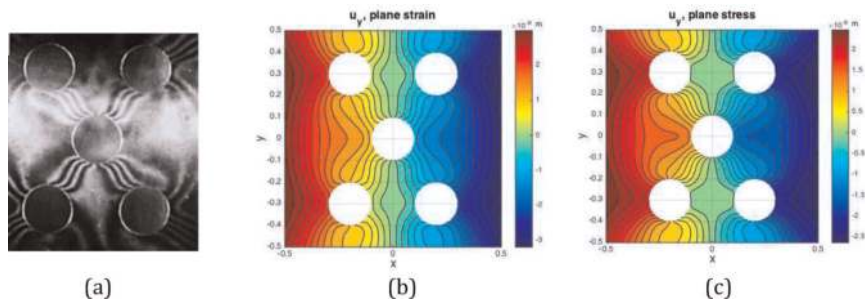


Figure 6. (a) $u_y(x,y)$ displacement magnitude contours [10]. (b) LSM plane strain solution for u_y (c) LSM plane stress solution for u_y .

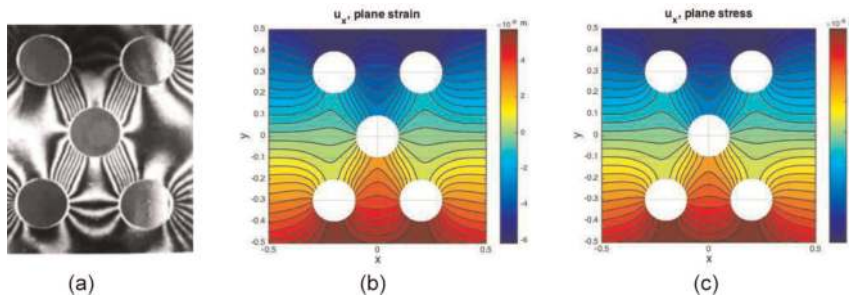


Figure 7. (a) $v(x,y)$ displacement magnitude contours [10]. (b) LSM plane strain solution for u_x . (c) LSM plane stress solution for u_x .

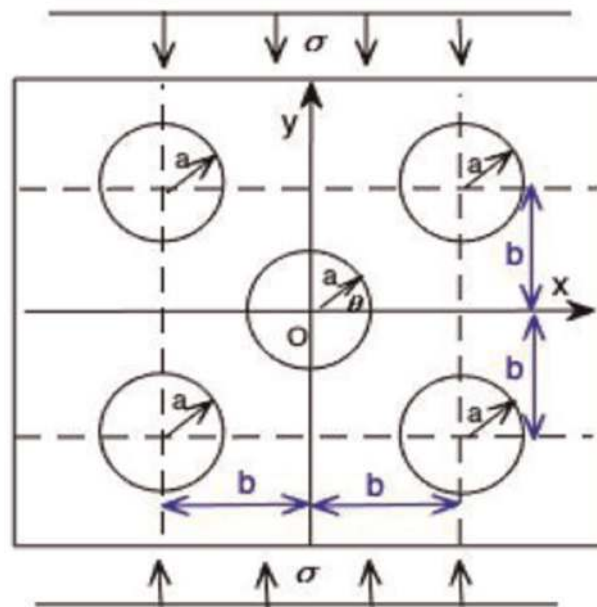


Figure 8. An infinite plate containing five equal circular holes under axial compressive stress ($b = 3\sqrt{2a}/2$ and $\sigma = 1$). No internal pressure load.

Figure 8, one can next compute the three polar strain tensor components using the following coordinate transformation for the strain tensor elements (e.g., Kelly Notes Solid Mechanics Part 2, Eq. 4.2.17):

$$\epsilon_r = \epsilon_{xx} \cos^2 \theta + \epsilon_{yy} \sin^2 \theta + \epsilon_{xy} \sin 2\theta \quad (39)$$

$$\epsilon_\theta = \epsilon_{xx} \sin^2 \theta + \epsilon_{yy} \cos^2 \theta - \epsilon_{xy} \sin 2\theta \quad (40)$$

$$\epsilon_{r\theta} = (\epsilon_{yy} - \epsilon_{xx}) \sin \theta \cos \theta + \epsilon_{xy} \cos 2\theta \quad (41)$$

Please note that for the un-pressurized hole subjected to (only) far-field stress, the radial strain, ϵ_r at the hole, the boundary will vanish (only at the hole boundary and not beyond).

Path 2: Revert to the original displacement equations in polar coordinates (Sections 2.1 to 2.5) and compute the displacement gradients in polar coordinates:

$$\varepsilon_r = \frac{\partial u_r}{\partial r} \quad (42)$$

$$\varepsilon_\theta = \frac{1}{r} \frac{\partial u_\theta}{\partial \theta} + \frac{u_r}{r} \quad (43)$$

$$\varepsilon_{r\theta} = \frac{1}{2} \left(\frac{1}{r} \frac{\partial u_r}{\partial \theta} + \frac{\partial u_\theta}{\partial r} - \frac{u_\theta}{r} \right) \quad (44)$$

After having obtained the polar displacement gradients, one may compute the stresses for a plane stress (thin plate) problem from the following constitutive equations:

$$\sigma_r = \frac{E}{1-\nu^2} (\varepsilon_r + \varepsilon_\theta \nu) \quad (45)$$

$$\sigma_\theta = \frac{E}{1-\nu^2} (\varepsilon_\theta + \varepsilon_r \nu) \quad (46)$$

$$\sigma_{r\theta} = \frac{E}{2(1+\nu)} \varepsilon_{r\theta} \quad (47)$$

For plane strain (thick plate) problem, the corresponding constitutive equations are ([32], Eq. (5-38)):

$$\sigma_r = \frac{2G}{1-2\nu} [(1-\nu) + \varepsilon_\theta \nu] = \frac{E}{(1+\nu)(1-2\nu)} [(1-\nu) + \varepsilon_\theta \nu] \quad (48)$$

$$\sigma_\theta = \frac{2G}{1-2\nu} [\varepsilon_\theta(1-\nu) + \varepsilon_r \nu] = \frac{E}{(1+\nu)(1-2\nu)} [\varepsilon_\theta(1-\nu) + \varepsilon_r \nu] \quad (49)$$

$$\sigma_{r\theta} = G\varepsilon_{r\theta} = \frac{E}{2(1+\nu)} \varepsilon_{r\theta} \quad (50)$$

For completeness, polar strain tensor components can be computed from the stress tensor components as follows ([32], Eq. (5-37)):

$$\varepsilon_r = \frac{1}{2G} [\sigma_r(1-\nu) - \sigma_\theta \nu] \quad (51)$$

$$\varepsilon_\theta = \frac{1}{2G} [\sigma_\theta(1-\nu) - \sigma_r \nu] \quad (52)$$

$$\varepsilon_{r\theta} = \frac{\sigma_{r\theta}}{G} \quad (53)$$

The polar strain tensor components can be converted to the Cartesian components at any one time using the polar coordinate transformations [e.g. [12], Eq. (48)]:

$$\varepsilon_{xx} = \varepsilon_r \cos^2 \theta + \varepsilon_\theta \sin^2 \theta \quad (54)$$

$$\varepsilon_{yy} = \varepsilon_r \sin^2\theta + \varepsilon_\theta \cos^2\theta \quad (55)$$

$$\varepsilon_{xy} = \frac{\varepsilon_r - \varepsilon_\theta}{2} \sin 2\theta \quad (56)$$

4.2.4 Case 2–2: results

The results of our benchmark test for Case 2–2, as per the methodology outlined above, are given here. First, a baseline solution for the tangential stress around a single hole (Case 1–1) is given in **Figure 9**. An important finding is that the plane stress solution for tangential stress concentrations around the hole is less sensitive to the Poisson’s ratio compared with the plane strain solution as shown in **Figure 9a, b**, and **Table 3** (for positive values of ν). This subtle difference has not been emphasized before. Overall, the delta between the plane strain and plane stress solutions becomes larger for larger Poisson’s ratios, resulting in the stress concentration factor being 3 for the plane stress boundary condition, increasing to nearly 4 for the plane strain boundary condition.

The impacts of the Poisson ratio and different boundary conditions were analyzed in more detail, based on the displacement fields quantified in Appendix C, which led to the following conclusions:

- Displacements in the x -direction are insensitive to the value of ν in case of plane stress.
- Displacements in the x -direction are slightly sensitive to the value of ν in case of plane strain.
- Displacements in the y -direction are sensitive to the value of ν in both plane strain and plane stress.

When the Poisson’s ratio is 0, the stress concentrations, according to our LSM models, are the same for plane stress and plane strain boundary conditions (**Figure 9a**). This matching in the concentrations at $\nu = 0$ between the plane stress and plane strain solutions can also be seen in Eq. (46), for plane stress, and Eq. (49), for plane strain. For the higher Poisson’s ratio $\nu = 0.3$, the plane strain

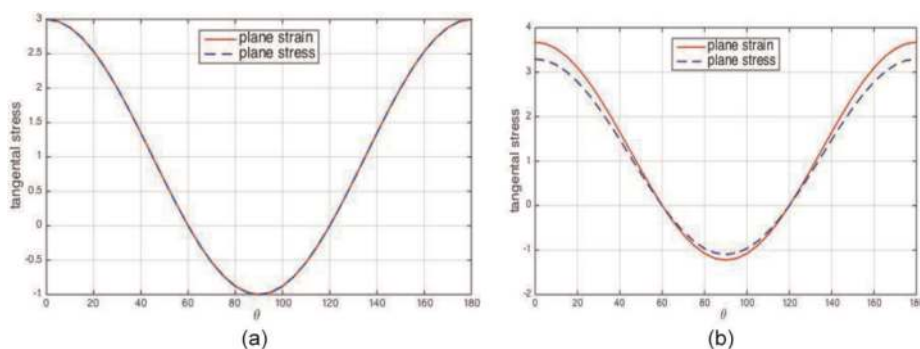


Figure 9. Tangential stress concentration variations around the rim of a single hole (case 1–1). (a) Poisson’s ratio $\nu = 0.0$, and (b) $\nu = 0.3$.

Poisson's ratio ν [-]	Plane strain		Plane stress	
	$\max_{0 \leq \theta \leq \pi} (\sigma_\theta)$	$\min_{0 \leq \theta \leq \pi} (\sigma_\theta)$	$\max_{0 \leq \theta \leq \pi} (\sigma_\theta)$	$\min_{0 \leq \theta \leq \pi} (\sigma_\theta)$
-0.5	3.3749	-1.1249	3.9999	-1.3333
-0.4	3.2666	-1.0888	3.5714	-1.1904
-0.3	3.1687	-1.0562	3.2967	-1.0989
-0.2	3.0857	-1.0285	3.1250	-1.0416
-0.1	3.0249	-1.0083	3.0303	-1.0101
0.0	3.0000	-1.0000	3.0000	-1.0000
0.1	3.0374	-1.0124	3.0303	-1.0101
0.2	3.1999	-1.0666	3.1250	-1.0416
0.3	3.6749	-1.2249	3.2967	-1.0989
0.4	5.4000	-1.8000	3.5714	-1.1904
0.5	INF	-INF	3.9999	-1.3333

Table 3. Maximum and minimum tangential stress (σ_θ) around the rim of the central hole in a single hole problem (case 1-1) corresponding to different values of Poisson's ratio ν . The max of σ_θ occurs at $\theta = 0$ and π . The minimum of σ_θ is at $\theta = \frac{\pi}{2}$.

solution starts to show a higher stress concentration than the plane stress solution (Figure 9b).

Next, we show the 5-hole (Case 2-2) stress concentrations around the central hole (Figure 10a, b). For the small Poisson's ratio of $\nu = 0$, stress concentrations of LSM solutions under plane strain and plane stress boundary conditions are identical (Figure 10a). However, for $\nu = 0.3$, the plane strain solution shows higher stress concentrations at locations $\theta = 0, \pi$ (Figure 10b) with a maximum value of 3.7728 corresponding to the maximum value for the plane stress solution 3.3481 (see Table 4). Overall, the minimum stress concentrations at $\theta = \pi/2$ approach -2 (due to stress interference effects between the central hole and its surrounding 4 holes). The maximum stress concentration at $\theta = 0, \pi$ is decreased from 3 (for a single hole with $\nu = 0$, Figure 9a) to 2.9695 (for 5-holes with $\nu = 0$, Figure 10a).

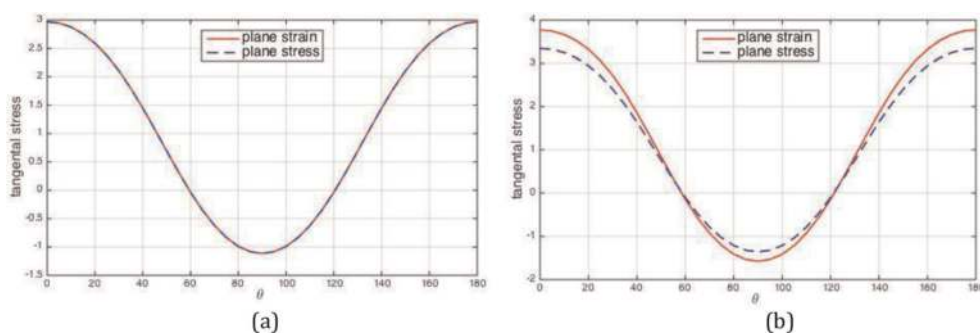


Figure 10. Tangential stress concentration variations around the rim of the central hole in a 5-hole problem (case 2-2). (a) Poisson's ratio $\nu = 0.0$, and (b) $\nu = 0.3$.

Poisson's ratio ν [-]	Plane strain		Plane stress	
	$\max_{0 \leq \theta \leq \pi} (\sigma_\theta)$	$\min_{0 \leq \theta \leq \pi} (\sigma_\theta)$	$\max_{0 \leq \theta \leq \pi} (\sigma_\theta)$	$\min_{0 \leq \theta \leq \pi} (\sigma_\theta)$
-0.5	3.2441	-1.0121	3.7877	-1.2170
-0.4	3.1534	-1.0876	3.4125	-1.1344
-0.3	3.0738	-1.0782	3.1783	-1.0913
-0.2	3.0102	-1.0765	3.0396	-1.0762
-0.1	2.9706	-1.0859	2.9735	-1.0842
0.0	2.9695	-1.1135	2.9695	-1.1135
0.1	3.0356	-1.1725	3.0255	-1.6531
0.2	3.2361	-1.2948	3.1469	-1.2435
0.3	3.7728	-1.5748	3.3481	-1.3559
0.4	5.6541	-2.4860	3.6577	-1.5167
0.5	INF	-INF	3.1310	-1.7523

Table 4. Maximum and minimum tangential stress (σ_θ) around the rim of the central hole in a 5-hole problem (case 2–2) corresponding to different values of Poisson's ratio ν . The max of σ_θ occurs at $\theta = 0$ and π . The minimum of σ_θ is at $\theta = \frac{\pi}{2}$.

Figure 11a and **b** include the prior solutions for the same 5-hole problem configuration using a numerical solution method in ref. [11] and Laurent series method in ref. [31]. Unfortunately, the Poisson's ratio is not specified by either [11] or [31]; neither was the boundary condition made explicit. However, **Figure 11a** shows that the plane strain solution is closer to [11, 31] results than the plane stress for $\nu = 0.3$, and for $\nu = 0.4$, the plane stress solution is closer than the plane strain. As for the photo-elastic comparison of Case 2–1, the prototype used in Case 2–2 has finite lateral width, due to which the LSM for a similar domain but based on an infinite plate solution will be progressively mismatching.

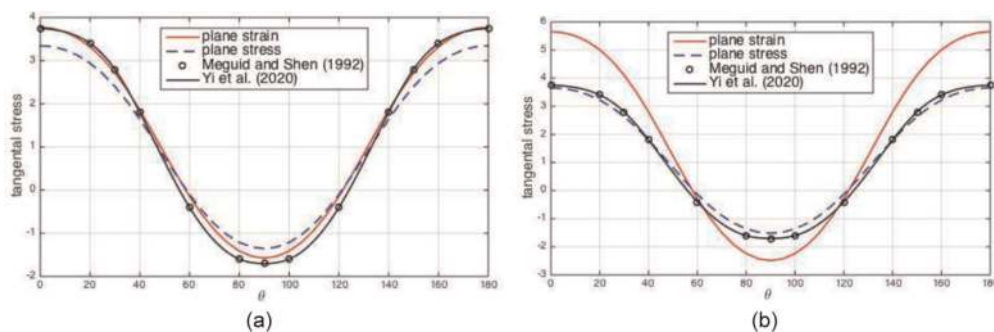


Figure 11. Comparison of the stress concentrations around the rim of the central hole in a 5-hole problem (case 2–2) using (1) LSM solutions (red line for plane strain and blue line for plane stress boundary conditions) and (2) the prior solutions for the same 5-hole problem configuration using a numerical solution method [11] (solid black line) and Laurent series method [31] (black circles). (a) Poisson's ratio $\nu = 0.3$, and (b) $\nu = 0.4$.

5. Discussion

Usually, convenient simplifications are adopted when we develop mathematical descriptions of a physical process, such as the elastic displacements due to boundary forces and internal discontinuities such as circular cylindrical perforations. Examples are the description of two extreme types of boundary conditions—plane stress (thin-plate approach) and plane strain (thick-plate approach).

In spite of these model simplifications, the results of the computations based on the thin- and thick-plate approaches are routinely used in many practical applications. However, the disparities between the model results and actual displacements in the natural prototype can rarely be evaluated in detail, but some theoretical extrapolations are still possible (see ref. [10] for some experimental methods).

The present study documents a careful evaluation of the delta's arising in resulting stress concentrations due to a prototype that would behave like a thick medium (plane strain boundary conditions) but is treated with a plane stress boundary condition solution (thin-plate medium). This treatment is basically due to applying Kirsch [1] solutions to quantify the stress concentration on the rim of the hole in a thick plate (where, σ_{zz} is locally zero likewise everywhere in the thin-plate case). Such loose application of boundary constraints routinely occurs in wellbore stability problems, as detailed in this paper.

This paper specifically discussed the relevance of our findings for borehole stability studies. Traditionally, wellbore stability computations are based on analytical solutions [1] for stresses near a hole in an elastic plate. The Kirsch [1] solution is valid for a plane stress boundary condition; this is a so-called thin-plate solution ($\frac{a}{h} \rightarrow \infty$), for which everywhere $\sigma_{zz} = 0$. The opposite end of the spectrum is a plane strain boundary condition (*i.e.*, $\epsilon_{zz} = 0$) or a thick plate ($\frac{a}{h} \rightarrow 0$) approach, where σ_{zz} is locally zero but in places may be either larger or smaller than zero, as has been quantified in Appendix C of our study. In our present study, we quantified, σ_{zz} , spatially everywhere normal to both a thick plate and thin plate with thickness $2h$, perforated by either single or multiple hole(s) of typical hole radius a (see Appendix C). Solutions were also given for cases with internal pressure loading.

According to the new results presented in our study, after evaluating the stress concentrations and transverse σ_{zz} for the perfect plane strain case ($\frac{a}{h} \rightarrow 0$) not only at the rim of the holes but everywhere in a finite domain around the hole(s), we can confirm that even for the most extreme case of plane strain (as opposed to plane stress, $\frac{a}{h} \rightarrow \infty$) where σ_z vanishes in all locations, the difference between the respective solutions remains minimal.

6. Conclusion

Our study articulates that, in fact, any real elastic medium with a finite thickness, for cases involving circular cylindrical holes (single or multiple), will behave in a way intermediate between the plane stress and plane strain end members. We have resorted to [14] scalar $\frac{a}{h}$ as a very useful metric to estimate where the real prototype with finite thickness occurs between the end-member solutions. For $\frac{a}{h} \ll 1$ and $\frac{a}{h} \rightarrow 0$, we have tiny holes in a very thick plate. Many prototypes of stress concentrations near boreholes in the geological subsurface will be adequately described by the plane strain boundary condition. For $\frac{a}{h} \gg 1$ and $\frac{a}{h} \rightarrow \infty$, we have large holes in a very thin plate, for which

prototypes exist in riveted wing panels for airplanes. Of course, there exists an unlimited range of prototypes that fall somewhere in between the extremes, and $\frac{a}{h}$ provides a metric to estimate how far the solution remains separated from the two end members.

Several specific cases have been analyzed in our study and we have quantified the delta of the displacements, strain, and stresses, as well as the Poisson's ratio for the two end-members (see Appendices to this study). Based on these specific cases, the following conclusions can be drawn (with emphasis on the delta's arising when applying either plane stress or plane strain approximate solutions):

- For multi-hole problems, we considered the 5-hole photo-elastic prototype shown in **Figure 4**. For this elastic prototype, the ratio between the holes' radii and the plate thickness is $\frac{a}{h} = 2$, which is theoretically closer to plane stress (thin plate) than to a plane strain (thick plate) boundary condition. The analytical LSM plane stress and plane strain solutions in **Figures 5–7(b, c)** along with the small deltas quantified in **Figure 5d** validate this theoretical deduction.
- We also analyzed the impact of the Poisson's ratio on the tangential stress concentrations around the central hole in a 5-hole problem surrounded by four symmetrically distributed circular holes (see **Figure 8**). We conclude that the plane strain solution is more sensitive to the Poisson's ratio than the plane stress solution. This different sensitivity increases the delta between plane strain and plane stress solutions for the tangential stress concentrations around the central hole when ν increases (**Figures 9 and 10**).
- The difference between the plane strain and plane stress solutions indicates that the prior solutions for the same 5-hole problem using a numerical solution method in ref. [11] and Laurent series method in ref. [31] were most likely for the plane strain boundary condition with $\nu = 0.3$, or possibly for plane stress with $\nu = 0.4$ (see **Figure 11**).
- For holes subjected to an internal pressure only, there is no delta between the plane stress and plane strain solutions of the principal stress distributions σ_1 and σ_2 ; the displacement fields will remain identical for both cases (see **Figure 2**).
- For a combination of far-field stress and the internal hole pressure, the displacements due to the internal pressure on the hole add lateral uniform volumetric displacements, effectively shifting the locations where the deltas occur (see **Figure 3**).

In a more general sense, the following was observed:

- Stress concentrations near tiny holes in a very thick plate approach the solution of plane stress boundary condition.
- Stress concentrations near large holes in a very thin plate approach the solution of plane strain boundary condition.
- For most practical cases, the response will be intermediate between the plane stress and plane strain end members, depending on the relative dimensions of the plate thickness and hole diameter.

- For holes subjected to an internal pressure only, there is no difference between the plane stress (thin-plate solution) and plane strain solutions (thick-plate solutions)
- For cases with far-field stress, the plane strain solution is more sensitive to the Poisson's ratio than the plane stress solution.

Acknowledgements

This research did not receive any specific grant from funding agencies in the public, commercial, or not-for-profit sectors. However, the authors acknowledge the generous support provided by the Department of Mathematics and the College of Petroleum Engineering & Geosciences (CPG) at King Fahd University of Petroleum & Minerals (KFUPM).

A. Validate the computational integrity of the plane strain displacement solutions of Section 2.2 using the plane stress solutions of Section 2.3

The plane strain solution, Eqs. (5) and (6), can be obtained directly from the plane stress solution, Eqs. (9) and (10), by replacing E with $E/(1 - \nu^2)$, and ν with $\nu/(1 - \nu)$ as follows:

Starting from the stress solution given by Eq. (9)

$$u_r = \sigma_{xx-\infty} \left(\frac{1 + \nu}{2Er} \right) \left\{ \frac{1 - \nu}{1 + \nu} r^2 + a^2 + \left(\frac{4a^2}{1 + \nu} + r^2 - \frac{a^4}{r^2} \right) \cos 2\theta \right\} \quad (A1)$$

and applying the above replacements we get

$$\begin{aligned} u_r &= \sigma_{xx-\infty} \left(\frac{1 + \left(\frac{\nu}{1 - \nu} \right)}{2 \left(\frac{E}{1 - \nu^2} \right) r} \right) \left\{ \frac{1 - \left(\frac{\nu}{1 - \nu} \right)}{1 + \left(\frac{\nu}{1 - \nu} \right)} r^2 + a^2 + \left(\frac{4a^2}{1 + \left(\frac{\nu}{1 - \nu} \right)} + r^2 - \frac{a^4}{r^2} \right) \cos 2\theta \right\} \\ &= \sigma_{xx-\infty} \left(\frac{1 + \nu}{2Er} \right) \left\{ (1 - 2\nu)r^2 + a^2 + \left(4a^2(1 - \nu) + r^2 - \frac{a^4}{r^2} \right) \cos 2\theta \right\} \\ &= \sigma_{xx-\infty} \left(\frac{1 + \nu}{2Er} \right) \left\{ r^2(1 - 2\nu + \cos 2\theta) + a^2 \left[1 + \left(4(1 - \nu) - \frac{a^2}{r^2} \right) \cos 2\theta \right] \right\} \end{aligned} \quad (A2)$$

Eq. (A2) represents the plan strain solution as given by Eq. (5). Similarly, one can obtain Eq. (6) from (10) using the same modification.

B. Converting the polar coordinate of the displacement field to the cartesian coordinate

B.1 Plane strain solution

Recall the plane strain solution for the hole with uniaxial far-field stress given by Eqs. (5) and (6)

$$u_r = \sigma_{xx-\infty} \left(\frac{1+v}{2Er} \right) \left\{ r^2(1-2v + \cos 2\theta) + a^2 \left[1 + \left(4(1-v) - \frac{a^2}{r^2} \right) \cos 2\theta \right] \right\} \quad (B1)$$

$$u_\theta = -\sigma_{xx-\infty} \left(\frac{1+v}{2Er} \right) \left[r^2 + a^2 \left(2(1-2v) + \frac{a^2}{r^2} \right) \right] \sin 2\theta \quad (B2)$$

Applying equations Eqs. (5) and (6) into

$$u_x = u_r \cos \theta - u_\theta \sin \theta, \quad u_y = u_r \sin \theta + u_\theta \cos \theta$$

we get,

$$u_x = \left[\sigma_{xx-\infty} \left(\frac{1+v}{2Er} \right) \{ r^2(1-2v + \cos 2\theta) \} \right] + a^2 \left[1 + \left(4(1-v) - \frac{a^2}{r^2} \right) \cos 2\theta \right] \cos \theta - \left[-\sigma_{xx-\infty} \left(\frac{1+v}{2Er} \right) \left[r^2 + a^2 \left(2(1-2v) + \frac{a^2}{r^2} \right) \right] \sin 2\theta \right] \sin \theta \quad (B3)$$

$$u_y = \left[\sigma_{xx-\infty} \left(\frac{1+v}{2Er} \right) \{ r^2(1-2v + \cos 2\theta) \} \right] + a^2 \left[1 + \left(4(1-v) - \frac{a^2}{r^2} \right) \cos 2\theta \right] \sin \theta + \left[-\sigma_{xx-\infty} \left(\frac{1+v}{2Er} \right) \left[r^2 + a^2 \left(2(1-2v) + \frac{a^2}{r^2} \right) \right] \sin 2\theta \right] \cos \theta \quad (B4)$$

Simplify Eqs. (B3) and (B4) and make use of the straightforward coordinate transformation formula:

$$x = r \cos \theta, \quad y = r \sin \theta, \quad r^2 = x^2 + y^2$$

to get the following

i. Before replacing $r^2 = x^2 + y^2$

$$u_x = \sigma_{xx-\infty} \left(\frac{1+v}{2Er} \right) \left\{ \left[r^2 \left(1-2v + \frac{x^2-y^2}{r^2} \right) + a^2 \left[1 + \left(4(1-v) - \frac{a^2}{r^2} \right) \frac{x^2-y^2}{r^2} \right] \right] \frac{x}{r} + \left[\left[r^2 + a^2 \left(2(1-2v) + \frac{a^2}{r^2} \right) \right] \frac{2xy}{r^2} \right] \frac{y}{r} \right\} = \sigma_{xx-\infty} \left(\frac{1+v}{2E} \right) \left\{ \left[r^2(1-2v) + x^2 - y^2 + a^2 + 4a^2(1-v) \left(\frac{x^2-y^2}{r^2} \right) - a^4 \left(\frac{x^2-y^2}{r^4} \right) \right] \frac{x}{r^2} + \left[2xy + (1-2v) \left(\frac{4a^2xy}{r^2} \right) + \frac{2a^4xy}{r^4} \right] \frac{y}{r^2} \right\} \quad (B5)$$

$$\begin{aligned}
 u_y &= \sigma_{xx-\infty} \left(\frac{1+v}{2Er} \right) \left\{ \left[r^2 \left(1 - 2\nu + \frac{x^2 - y^2}{r^2} \right) + a^2 \left[1 + \left(4(1-\nu) - \frac{a^2}{r^2} \right) \frac{x^2 - y^2}{r^2} \right] \right] \frac{y}{r} \right. \\
 &\quad \left. - \left[\left[r^2 + a^2 \left(2(1-2\nu) + \frac{a^2}{r^2} \right) \right] \frac{2xy}{r^2} \right] \frac{x}{r} \right\} \\
 &= \sigma_{xx-\infty} \left(\frac{1+v}{2E} \right) \left\{ \left[r^2(1-2\nu) + x^2 - y^2 + a^2 + 4a^2(1-\nu) \left(\frac{x^2 - y^2}{r^2} \right) \right. \right. \\
 &\quad \left. \left. - a^4 \left(\frac{x^2 - y^2}{r^4} \right) \right] \frac{y}{r^2} - \left[2xy + (1-2\nu) \left(\frac{4a^2xy}{r^2} \right) + \frac{2a^4xy}{r^4} \right] \frac{x}{r^2} \right\} \quad (B6)
 \end{aligned}$$

ii. After replacing $r^2 = x^2 + y^2$

$$\begin{aligned}
 u_x &= \sigma_{xx-\infty} \left(\frac{1+v}{2E} \right) \left\{ \left[(x^2 + y^2)(1-2\nu) + x^2 - y^2 + a^2 + 4a^2(1-\nu) \left(\frac{x^2 - y^2}{x^2 + y^2} \right) \right. \right. \\
 &\quad \left. \left. - a^4 \left(\frac{x^2 - y^2}{(x^2 + y^2)^2} \right) \right] \left(\frac{x}{x^2 + y^2} \right) + \left[2xy + (1-2\nu) \left(\frac{4a^2xy}{x^2 + y^2} \right) + \frac{2a^4xy}{(x^2 + y^2)^2} \right] \left(\frac{y}{x^2 + y^2} \right) \right\} \quad (B7)
 \end{aligned}$$

$$\begin{aligned}
 u_y &= \sigma_{xx-\infty} \left(\frac{1+v}{2E} \right) \left\{ \left[(x^2 + y^2)(1-2\nu) + x^2 - y^2 + a^2 + 4a^2(1-\nu) \left(\frac{x^2 - y^2}{x^2 + y^2} \right) \right. \right. \\
 &\quad \left. \left. - a^4 \left(\frac{x^2 - y^2}{(x^2 + y^2)^2} \right) \right] \left(\frac{y}{x^2 + y^2} \right) - \left[2xy + (1-2\nu) \left(\frac{4a^2xy}{x^2 + y^2} \right) + \frac{2a^4xy}{(x^2 + y^2)^2} \right] \left(\frac{x}{x^2 + y^2} \right) \right\} \quad (B8)
 \end{aligned}$$

B.2 Delta between plane strain and plane stress solutions

Applying equations Eqs. (11) and (12) into

$$u_x = u_r \cos \theta - u_\theta \sin \theta, \quad u_y = u_r \sin \theta + u_\theta \cos \theta$$

we get

$$\begin{aligned}
 u_x &= \left(-\sigma_{xx-\infty} \left(\frac{v^2}{Er} \right) (r^2 + 2a^2 \cos 2\theta) \right) \cos \theta - \left(\sigma_{xx-\infty} \left(\frac{v^2}{Er} \right) (2a^2 \sin 2\theta) \right) \sin \theta \\
 &= -\sigma_{xx-\infty} \left(\frac{v^2}{Er} \right) [(r^2 + 2a^2 \cos 2\theta) \cos \theta + (2a^2 \sin 2\theta) \sin \theta] \\
 &= -\sigma_{xx-\infty} \left(\frac{v^2}{E(x^2 + y^2)} \right) \left[\left(x^2 + y^2 + 2a^2 \frac{x^2 - y^2}{x^2 + y^2} \right) x + \left(4a^2 \frac{xy}{x^2 + y^2} \right) y \right] \quad (B9)
 \end{aligned}$$

and

$$\begin{aligned}
 u_y &= \left(-\sigma_{xx-\infty} \left(\frac{v^2}{Er} \right) (r^2 + 2a^2 \cos 2\theta) \right) \sin \theta + \left(\sigma_{xx-\infty} \left(\frac{v^2}{Er} \right) (2a^2 \sin 2\theta) \right) \cos \theta \\
 &= -\sigma_{xx-\infty} \left(\frac{v^2}{Er} \right) [(r^2 + 2a^2 \cos 2\theta) \sin \theta - (2a^2 \sin 2\theta) \cos \theta] \\
 &= -\sigma_{xx-\infty} \left(\frac{v^2}{E(x^2 + y^2)} \right) \left[\left(x^2 + y^2 + 2a^2 \frac{x^2 - y^2}{x^2 + y^2} \right) y - \left(4a^2 \frac{xy}{x^2 + y^2} \right) x \right] \quad (B10)
 \end{aligned}$$

We, also, can obtain Eqs. (B9) and (B10) by subtracting the Cartesian equations of the plane strain and the plane stress as follows:

$$\begin{aligned}
 u_x &= \sigma_{xx-\infty} \left(\frac{1+v}{2E} \right) \left\{ \left[(x^2 + y^2)(1 - 2v) + x^2 - y^2 + a^2 + 4a^2(1 - v) \left(\frac{x^2 - y^2}{x^2 + y^2} \right) \right. \right. \\
 &\quad \left. \left. - a^4 \left(\frac{x^2 - y^2}{(x^2 + y^2)^2} \right) \right] \left(\frac{x}{x^2 + y^2} \right) + \left[2xy + (1 - 2v) \left(\frac{4a^2 xy}{x^2 + y^2} \right) + \frac{2a^4 xy}{(x^2 + y^2)^2} \right] \left(\frac{y}{x^2 + y^2} \right) \right\} \\
 &\quad - \sigma_{xx-\infty} \left(\frac{1+v}{2E} \right) \left\{ \left[\frac{1-v}{1+v} (x^2 + y^2) + a^2 + \left(\frac{4a^2}{1+v} + x^2 + y^2 - \frac{a^4}{x^2 + y^2} \right) \left(\frac{x^2 - y^2}{x^2 + y^2} \right) \right] \right. \\
 &\quad \left. \times \left(\frac{x}{x^2 + y^2} \right) + \left[\left(\frac{1-v}{1+v} 2a^2 + x^2 + y^2 + \frac{a^4}{x^2 + y^2} \right) \left(\frac{2xy}{x^2 + y^2} \right) \right] \left(\frac{y}{x^2 + y^2} \right) \right\} \\
 &= \sigma_{xx-\infty} \left(\frac{1+v}{2E} \right) \left\{ \left[(x^2 + y^2)(1 - 2v) + x^2 - y^2 + a^2 + 4a^2(1 - v) \left(\frac{x^2 - y^2}{x^2 + y^2} \right) \right. \right. \\
 &\quad \left. \left. - a^4 \left(\frac{x^2 - y^2}{(x^2 + y^2)^2} \right) \right] \left(\frac{x}{x^2 + y^2} \right) + \left[2xy + (1 - 2v) \left(\frac{4a^2 xy}{x^2 + y^2} \right) + \frac{2a^4 xy}{(x^2 + y^2)^2} \right] \left(\frac{y}{x^2 + y^2} \right) \right. \\
 &\quad \left. - \left[\frac{1-v}{1+v} (x^2 + y^2) + a^2 + \left(\frac{4a^2}{1+v} + x^2 + y^2 - \frac{a^4}{x^2 + y^2} \right) \left(\frac{x^2 - y^2}{x^2 + y^2} \right) \right] \left(\frac{x}{x^2 + y^2} \right) \right. \\
 &\quad \left. - \left[\left(\frac{1-v}{1+v} 2a^2 + x^2 + y^2 + \frac{a^4}{x^2 + y^2} \right) \left(\frac{2xy}{x^2 + y^2} \right) \right] \left(\frac{y}{x^2 + y^2} \right) \right\} \\
 &= \sigma_{xx-\infty} \left(\frac{1+v}{2E} \right) \left\{ \left[(x^2 + y^2) \left(1 - 2v - \frac{1-v}{1+v} \right) + x^2 - y^2 - (x^2 + y^2) \left(\frac{x^2 - y^2}{x^2 + y^2} \right) \right. \right. \\
 &\quad \left. \left. + a^2 - a^2 + 4a^2(1 - v) \left(\frac{x^2 - y^2}{x^2 + y^2} \right) - a^4 \left(\frac{x^2 - y^2}{(x^2 + y^2)^2} \right) + \left(\frac{a^4}{x^2 + y^2} \right) \left(\frac{x^2 - y^2}{x^2 + y^2} \right) \right. \right. \\
 &\quad \left. \left. - \left(\frac{4a^2}{1+v} \right) \left(\frac{x^2 - y^2}{x^2 + y^2} \right) \right] \left(\frac{x}{x^2 + y^2} \right) + \left[2xy - (x^2 + y^2) \left(\frac{2xy}{x^2 + y^2} \right) + (1 - 2v) \left(\frac{4a^2 xy}{x^2 + y^2} \right) \right. \right. \\
 &\quad \left. \left. - \frac{1-v}{1+v} 2a^2 \left(\frac{2xy}{x^2 + y^2} \right) + \frac{2a^4 xy}{(x^2 + y^2)^2} - \left(\frac{a^4}{x^2 + y^2} \right) \left(\frac{2xy}{x^2 + y^2} \right) \right] \left(\frac{y}{x^2 + y^2} \right) \right\}
 \end{aligned}$$

$$\begin{aligned}
 &= \sigma_{xx-\infty} \left(\frac{1+v}{2E} \right) \left\{ \left[(x^2 + y^2) \left(1 - 2v - \frac{1-v}{1+v} \right) + 4a^2 \left(1 - v - \frac{1}{1+v} \right) \left(\frac{x^2 - y^2}{x^2 + y^2} \right) \right] \right. \\
 &\quad \left. \left(\frac{x}{x^2 + y^2} \right) + \left[(1 - 2v) \left(\frac{4a^2 xy}{x^2 + y^2} \right) - \frac{1-v}{1+v} 2a^2 \left(\frac{2xy}{x^2 + y^2} \right) \right] \left(\frac{y}{x^2 + y^2} \right) \right\} \\
 &= \sigma_{xx-\infty} \left(\frac{1+v}{2E} \right) \left\{ \left[(x^2 + y^2) \left(1 - 2v - \frac{1-v}{1+v} \right) \right. \right. \\
 &\quad \left. \left. + 4a^2 \left(1 - v - \frac{1}{1+v} \right) \left(\frac{x^2 - y^2}{x^2 + y^2} \right) \right] \left(\frac{x}{x^2 + y^2} \right) \right. \\
 &\quad \left. + \left[\left(1 - 2v - \frac{1-v}{1+v} \right) \left(\frac{4a^2 xy}{x^2 + y^2} \right) \right] \left(\frac{y}{x^2 + y^2} \right) \right\} \\
 &= \sigma_{xx-\infty} \left(\frac{1+v}{2E} \right) \left\{ \left[(x^2 + y^2) \left(\frac{1+v - 2v - 2v^2 - 1 + v}{1+v} \right) \right. \right. \\
 &\quad \left. \left. + 4a^2 \left(\frac{1+v - v - v^2 - 1}{1+v} \right) \left(\frac{x^2 - y^2}{x^2 + y^2} \right) \right] \left(\frac{x}{x^2 + y^2} \right) \right. \\
 &\quad \left. + \left[\left(\frac{1+v - 2v - 2v^2 - 1 + v}{1+v} \right) \left(\frac{4a^2 xy}{x^2 + y^2} \right) \right] \left(\frac{y}{x^2 + y^2} \right) \right\} \\
 &= \sigma_{xx-\infty} \left(\frac{1+v}{2E} \right) \left\{ \left[(x^2 + y^2) \left(\frac{-2v^2}{1+v} \right) + 4a^2 \left(\frac{-v^2}{1+v} \right) \left(\frac{x^2 - y^2}{x^2 + y^2} \right) \right] \left(\frac{x}{x^2 + y^2} \right) \right. \\
 &\quad \left. + \left[\left(\frac{-2v^2}{1+v} \right) \left(\frac{4a^2 xy}{x^2 + y^2} \right) \right] \left(\frac{y}{x^2 + y^2} \right) \right\} \\
 &= \sigma_{xx-\infty} \left(\frac{-2v^2}{2E} \right) \left\{ \left[(x^2 + y^2) + 2a^2 \left(\frac{x^2 - y^2}{x^2 + y^2} \right) \right] \left(\frac{x}{x^2 + y^2} \right) + \left[\left(\frac{4a^2 xy}{x^2 + y^2} \right) \right] \left(\frac{y}{x^2 + y^2} \right) \right\} \\
 &= -\sigma_{xx-\infty} \left(\frac{v^2}{E(x^2 + y^2)} \right) \left\{ \left[(x^2 + y^2) + 2a^2 \left(\frac{x^2 - y^2}{x^2 + y^2} \right) \right] x + \left[\left(\frac{4a^2 xy}{x^2 + y^2} \right) \right] y \right\} \\
 &= \text{(B9)}
 \end{aligned}$$

Following the same steps, we can obtain Eq. (B10).

C. Single hole analysis

Comprehensive results are given here for the vector displacement fields, strain tensor components, principal strains, stress tensor components, and principal stresses. The first column images are for plane strain; the second column images are for plane stress; and the third column quantifies the delta between plane strain and plane stress solutions. We will consider the three cases presented in Section 4.1 for the elastic plate model with a central single hole.

- Case 1-1: a far-field stress only,
- Case 1-2: an internal pressure only,
- Case 1-3: the superposed Cases 1-1 and 1-2.

C.1 Single-hole subject to far-field stress (Case 1-1)

1. Displacement fields

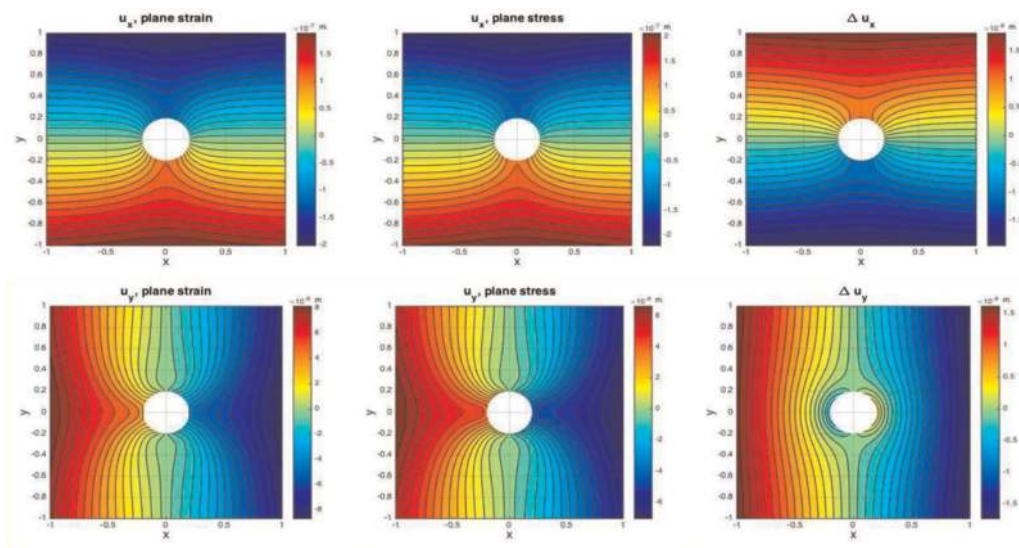


Figure C1. Complete results of the elastic displacement solutions around single hole in an elastic plate subjected to far-field stress. First column is for the plan strain solution given by Eqs. (15) and (16). Second column is the plane stress solution given by Eqs. (17) and (18). Third column quantifies the delta (difference) between plane strain and plane stress solutions using Eqs. (25) and (26).

2. Strain tensor components.

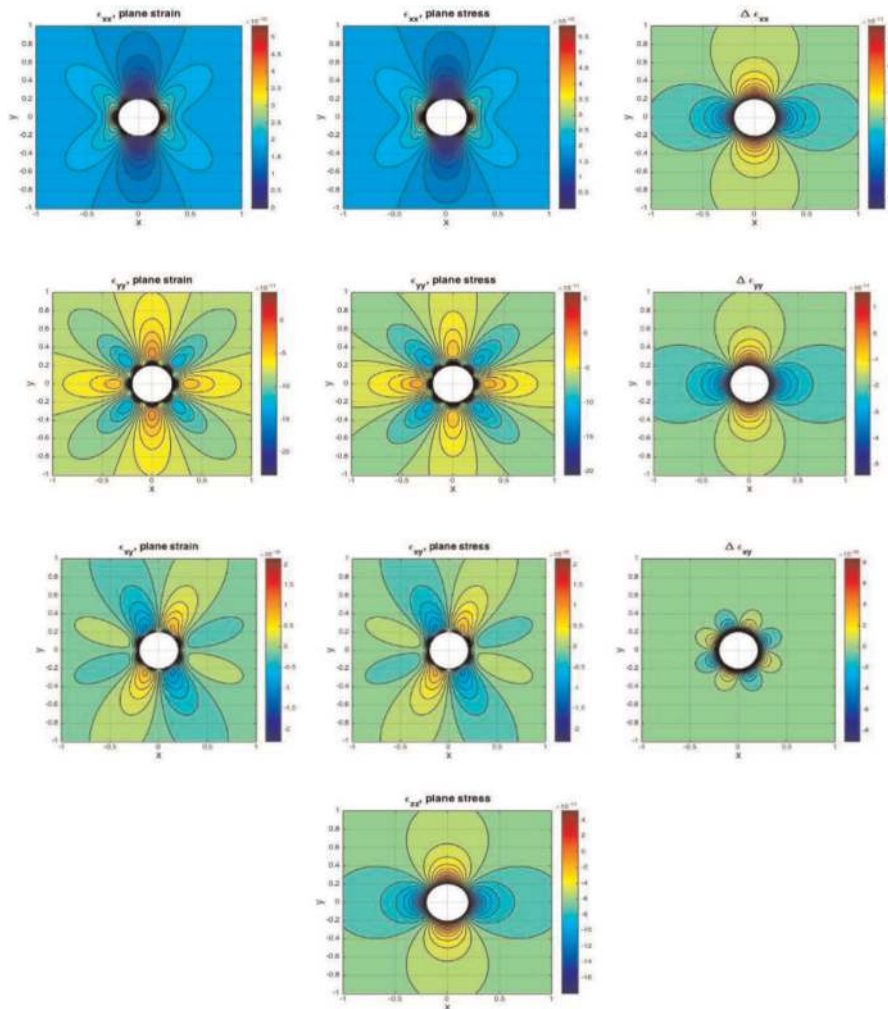


Figure C2. Strain tensor components around the single hole in an elastic plate subjected to far-field stress. First column is for the plan strain solution. Second column is the plane stress solution. Third column quantifies the delta (difference) between plane strain and plane stress solutions. These solutions are obtained by analytical differentiation of the displacement components in **Figure C1** in both x and y directions. See Eqs. (29)–(31) Note that $\epsilon_{zz} = 0$ for the plane strain solution and therefore there is no delta in z -direction.

3. Principal strains.

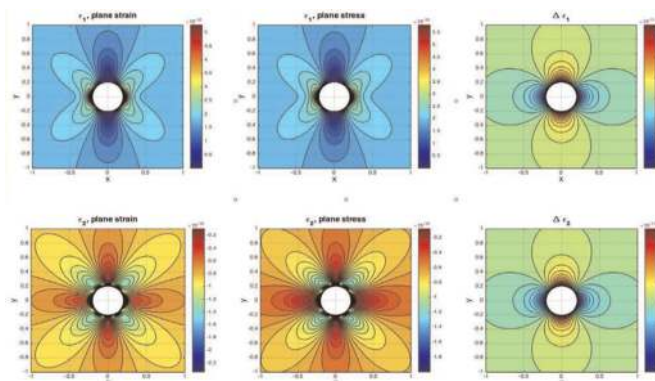


Figure C3. Principles strains around the single hole in an elastic plate subjected to far-field stress. These solutions are obtained by applying Eq. (36) for the principal strain magnitude solution using the strain tensors in **Figure C2**.

4. Stress tensor components.

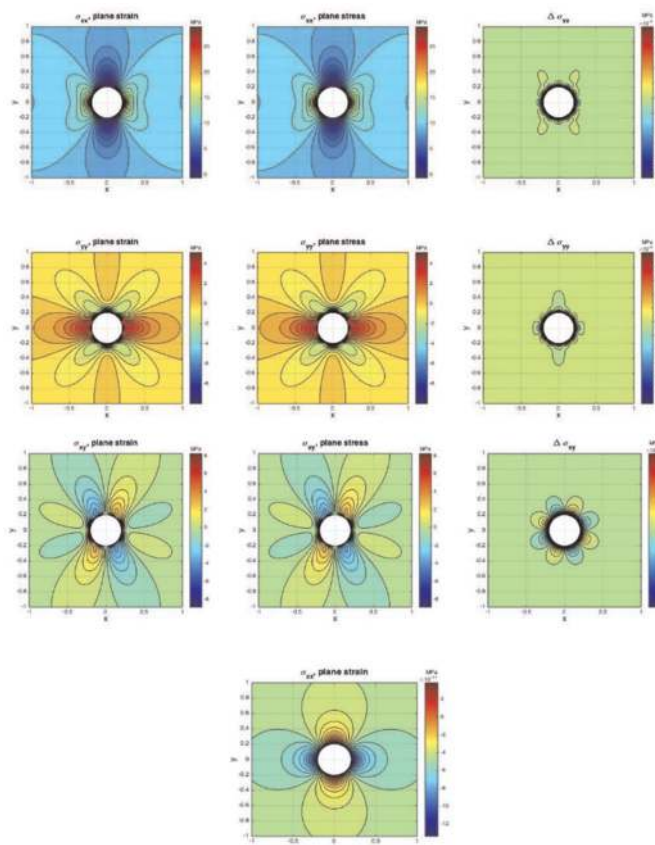


Figure C4. Stress tensor components around the single hole in an elastic plate subjected to far-field stress. First column is for the plan strain solution. Second column is the plane stress solution. Third column quantifies the delta (difference) between plane strain and plane stress solutions. These solutions are obtained from the relations between the strain tensor components and the stress tensor components shown in Eqs. (32)–(34). Note that $\sigma_{zz} = 0$ for plane stress solution and therefore there is no delta in the z -direction.

5. Principal stresses.

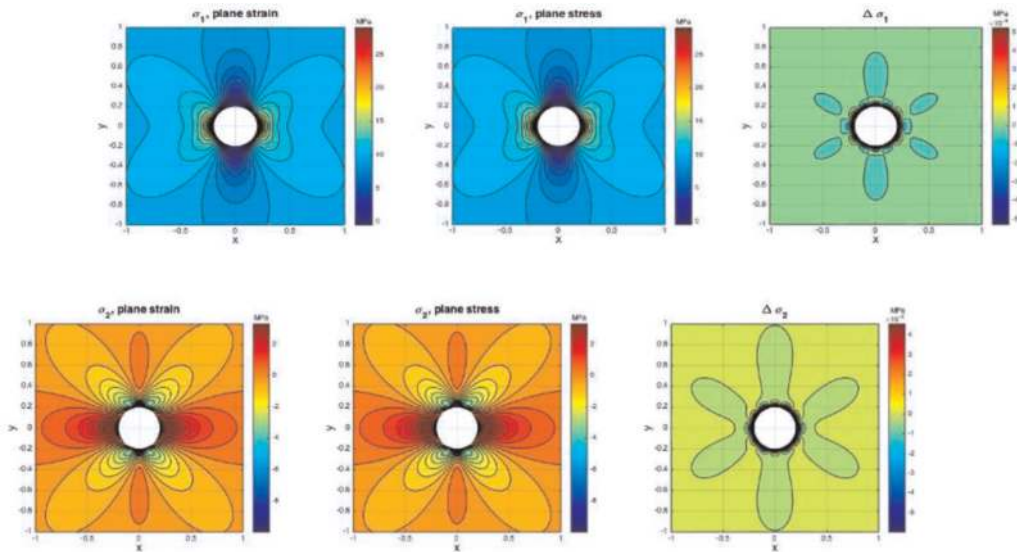


Figure C5. Principal stresses around the single hole in an elastic plate subjected to far-field stress. These solutions are obtained by applying Eqs. (37) and (38) using the tensor stress components in Figures C4.

6. Displacement field with respect to different values of Poisson's ratio.

In **Figures C5** and **C6**, we show the impact of the Poisson's ratio on the plane strain and plane stress displacement considering the model Case 1–1 of the elastic plate with a single hole. The model inputs are fixed as given in **Table 1** except for the Poisson's ratio that takes three different values $\nu = 0, 0.2, \text{ and } 0.4$. We can see from **Figure C6** the following results (as presented before in Case 2–2 results):

- i. Displacements in the x-direction are insensitive to the value of ν in case of plane stress.
- ii. Displacements in the x-direction are little bit sensitive to the value of ν in case of plane strain.
- iii. Displacements in the y-direction are sensitive to the value of ν in both plane strain and plane stress.

Therefore, this impact will extend to the resulting plane strain and plane stress solutions for the strain and stress tensor components computed based on the displacement results. This impact can be also generalized to the model of the elastic plate with 5-holes presented in Case 2–2. **Tables 3** and **4** illustrate, numerically, the impact of Poisson's ratio on the maximum and minimum values of the tangential stress (σ_θ) around the rim of the central hole in model Case 1–1 and model Case 2–2, respectively.

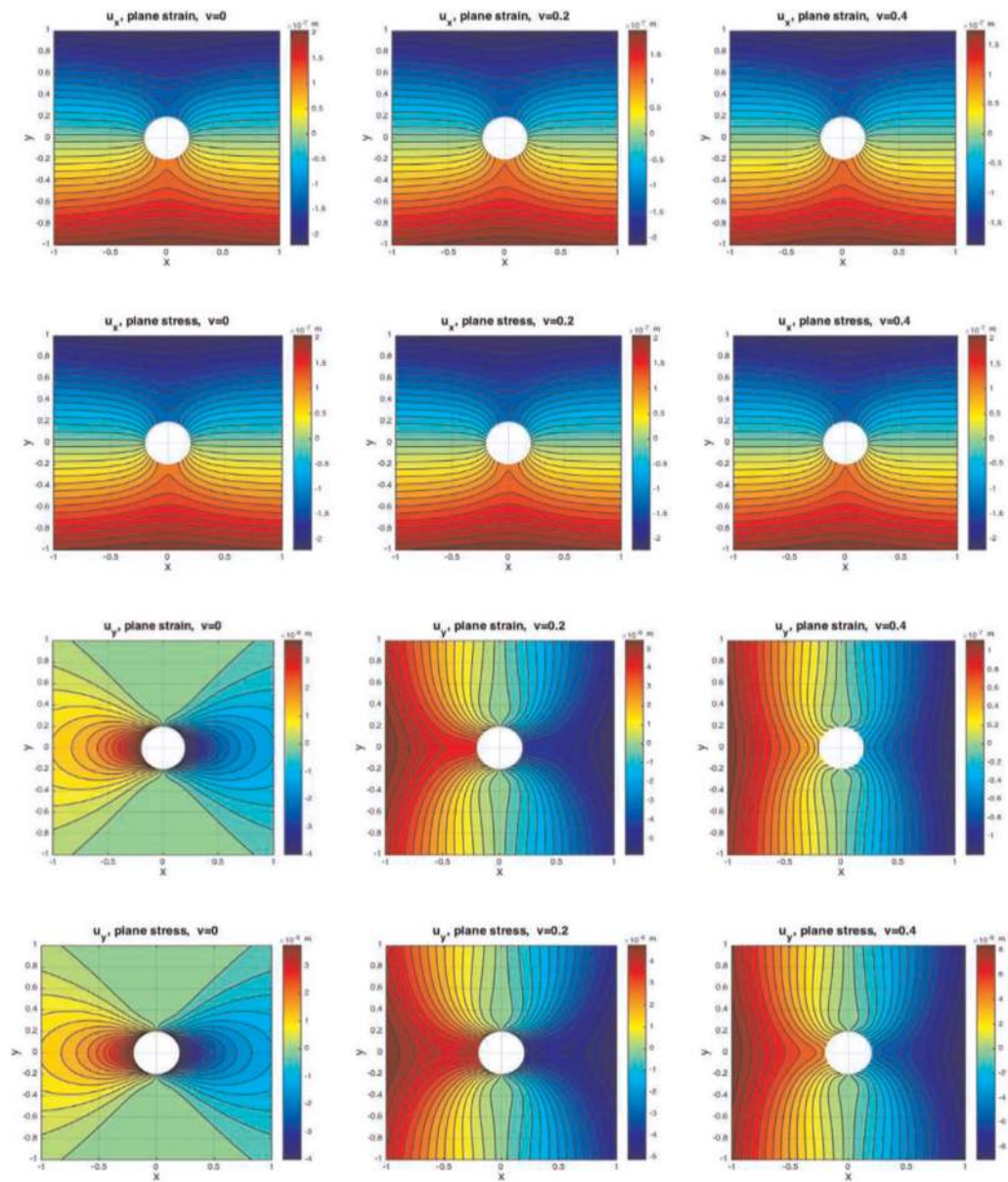


Figure C6. The plane strain and plane stress displacement solutions against different values of Poisson's ratio: $\nu = 0$ first column, $\nu = 0.2$ second column, and $\nu = 0.4$ third column. The first two rows are for the displacement in x -direction and the last two rows are for the displacement in y -direction.

C.2 Single-hole subject to the internal hole pressure (Case 1–2)

1. Displacement fields.

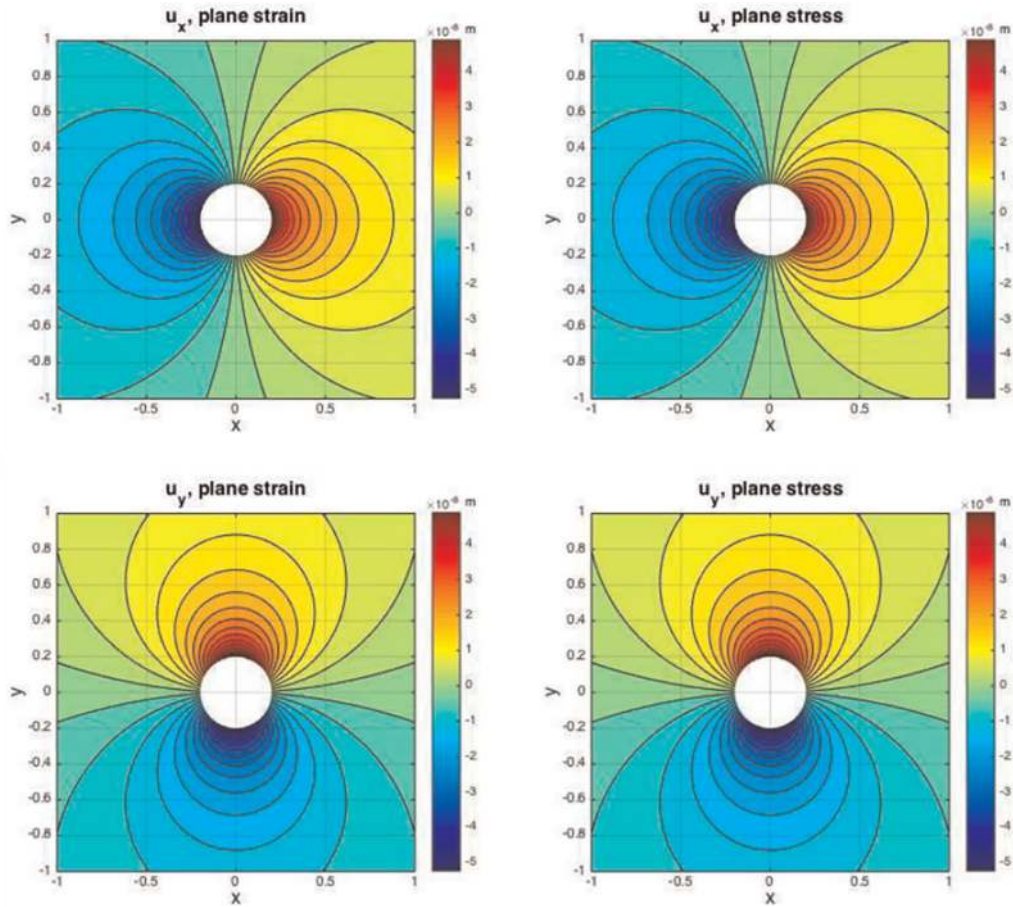


Figure C7.

Complete results of the elastic displacement solutions around the single hole in an elastic plate subjected to internal pressure. First column is for the plan strain solution. Second column is the plane stress solution. In the case when the elastic plate is subjected to internal pressure only, the plane strain and plane stress are identical and given by Eqs. (27) and (28). Therefore, there is no delta in this case. As in Case1–1 input parameters are listed in Table 1.

2. Strain tensor components.

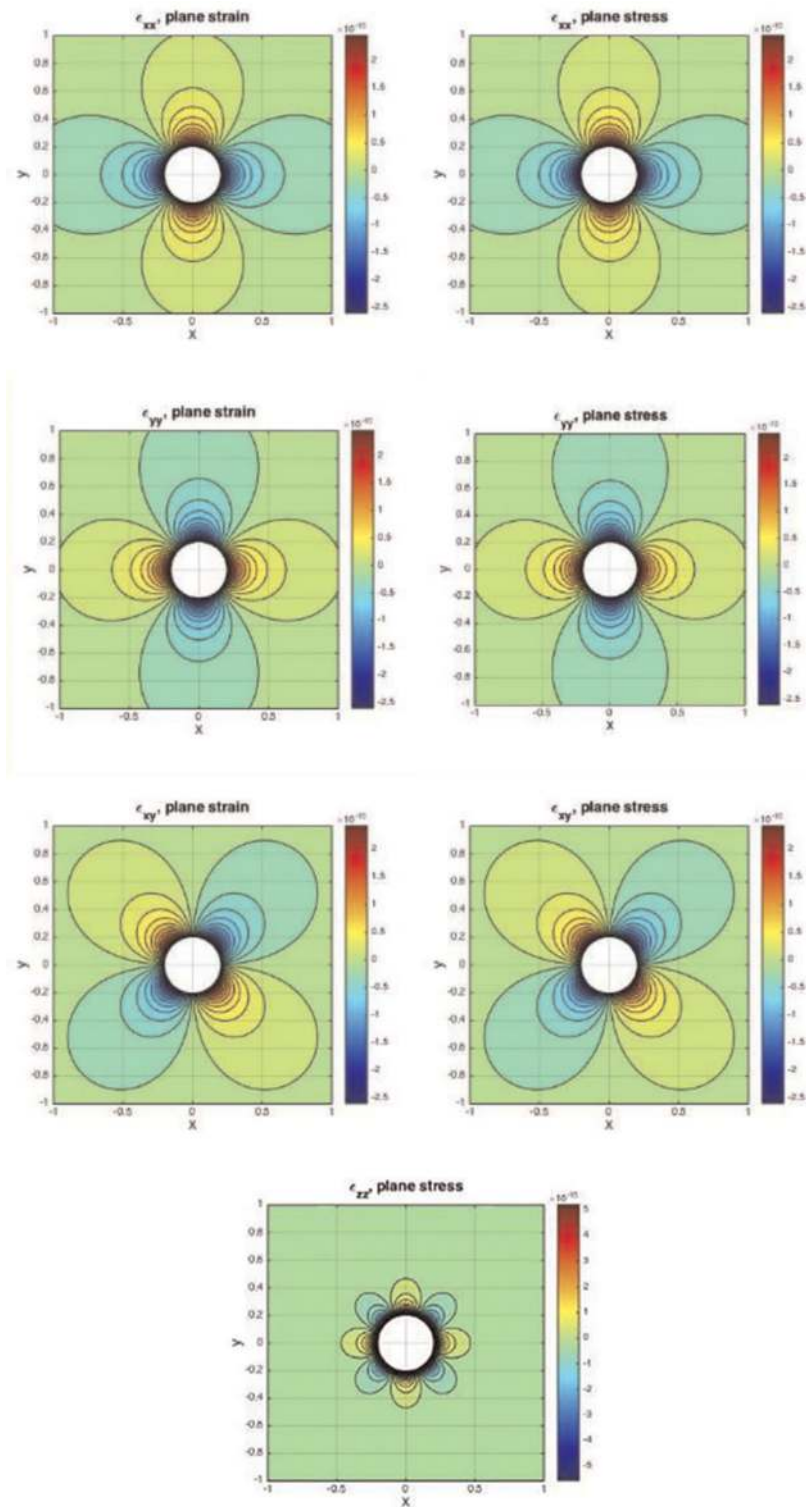


Figure C8. Strain tensor components around the single hole in an elastic plate subjected to internal pressure. First column is for the plan strain solution. Second column is the plane stress solution. These solutions are obtained by analytical differentiation of the displacement components in **Figure C7** in both x and y directions.

3. Principal strains.

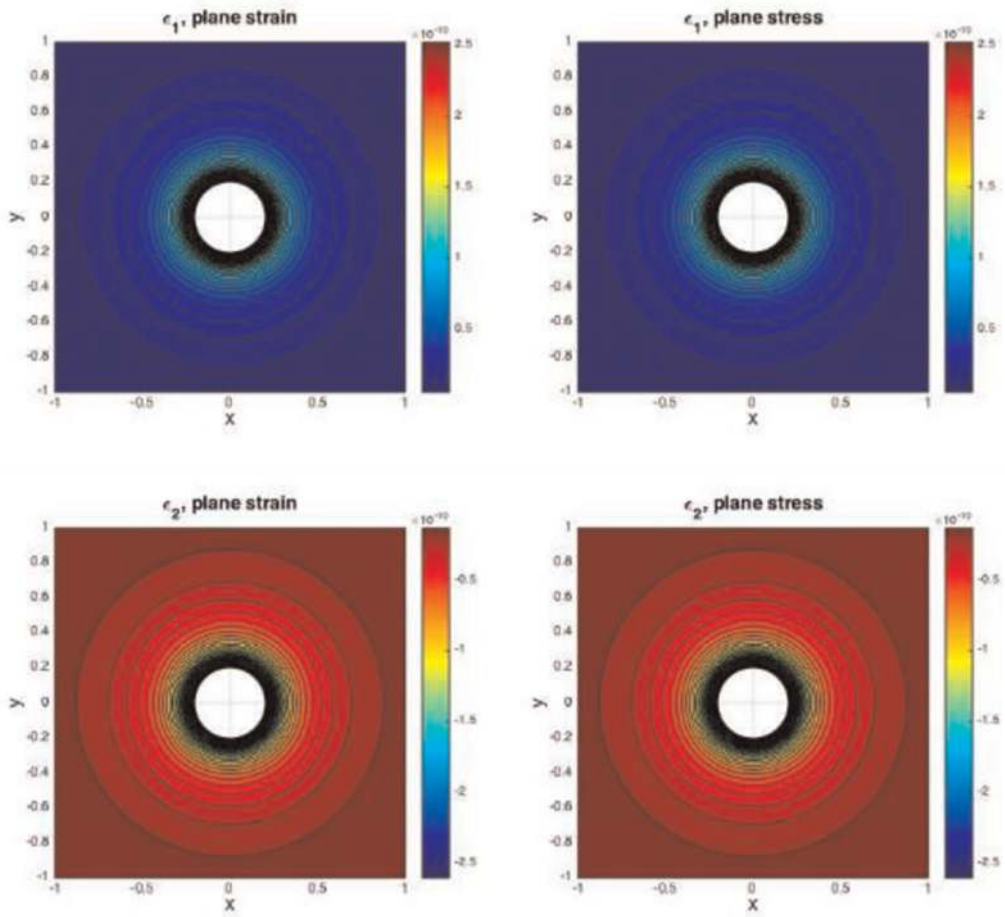


Figure C9. Principles strains around the single hole in an elastic plate subjected to internal pressure. These solutions are obtained by applying Eqs. (36) for the principal strain magnitude solution using the strain tensors in Figure C8.

4. Stress tensor components.

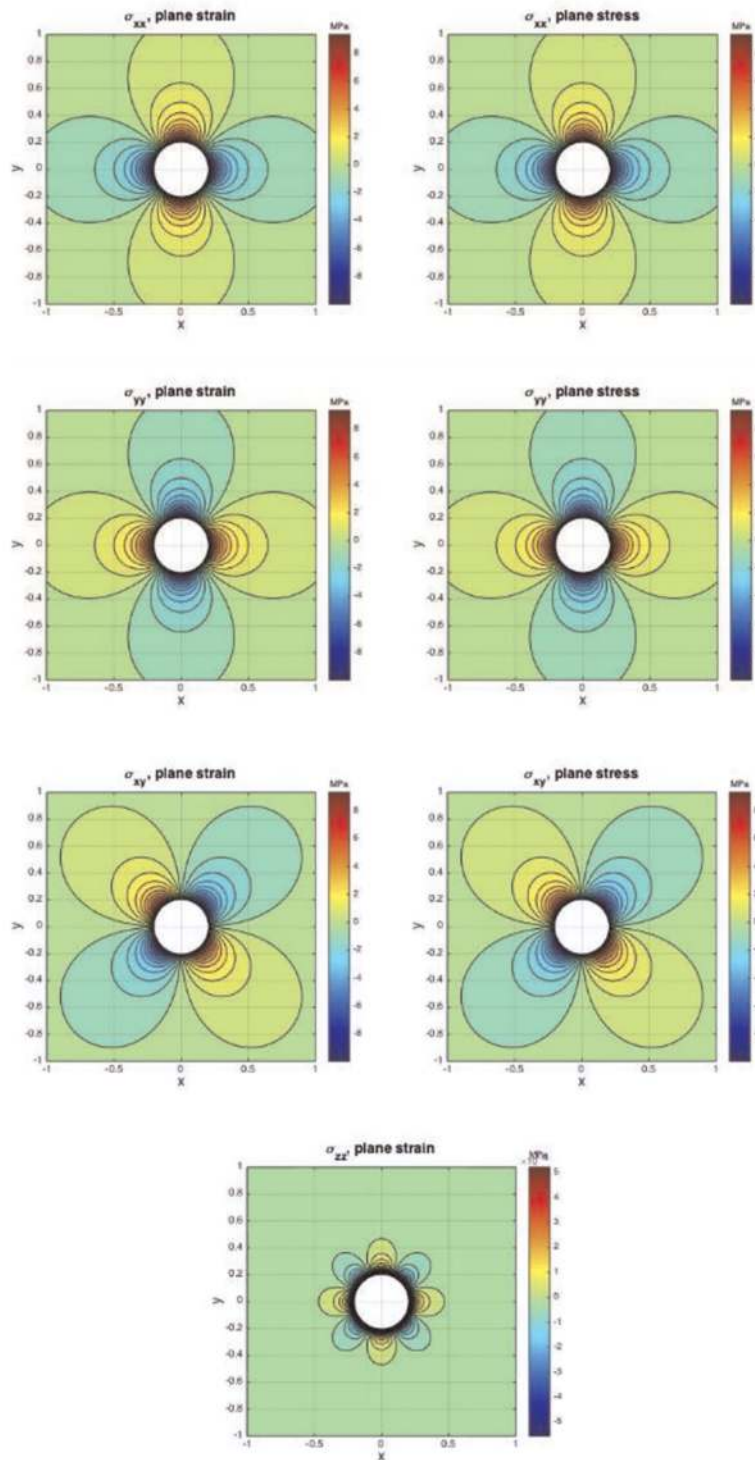


Figure C10. Stress tensor components around the single hole in an elastic plate subjected to internal pressure. First column is for the plane strain solution. Second column is the plane stress solution. These solutions are obtained from the relations between the strain tensor components and the stress tensor components shown in Eqs. (32)–(34).

5. Principal stresses.

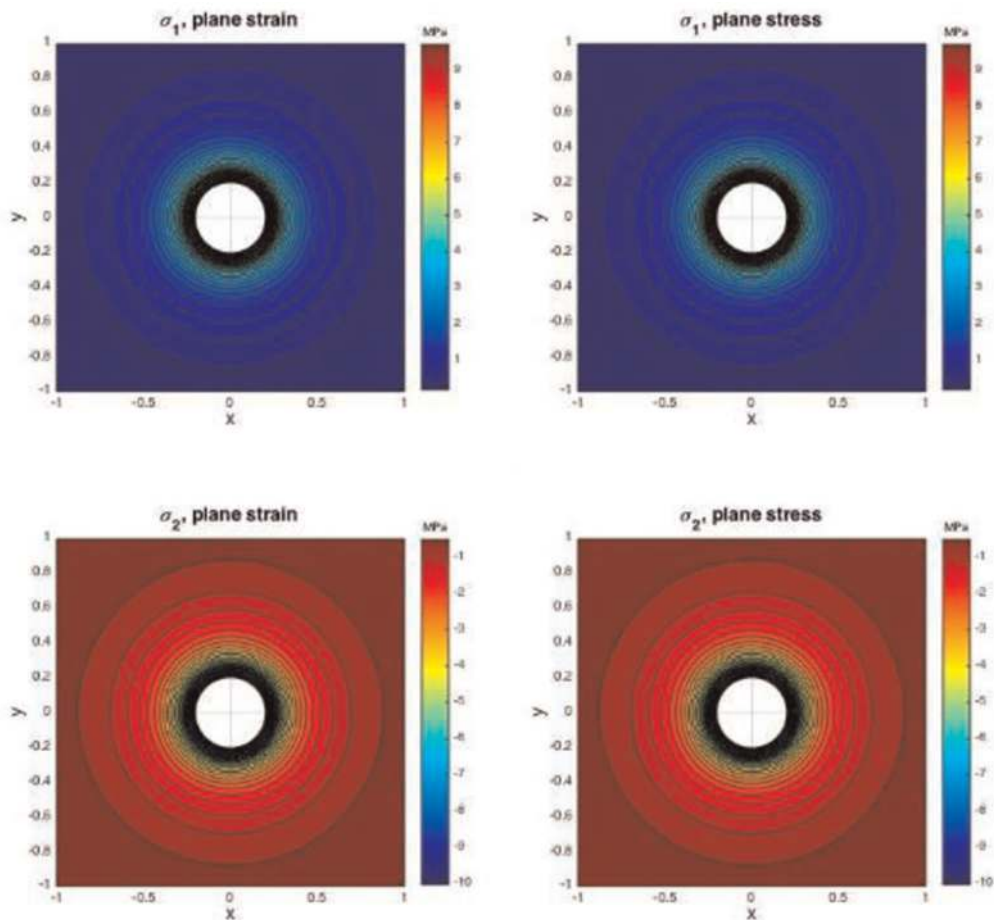


Figure C11. Principal stresses around the single hole in an elastic plate subjected to internal pressure. These solutions are obtained by applying Eqs. (37) and (38) using the tensor stress components in Figure C10.

C.3 The superposed Cases 1–1 and 1–2 (Case 1–3)

In this section, we consider Case 1–3 of the superposed of Cases 1–1 and 1–2. The plane strain displacement solutions in both directions are the sum of Eqs. (15), (16) and (27), (28). Similarly, the plane stress displacement solutions in both directions are the sum of Eqs. (17) and (18) and (27), (28). The strain tensor components, principal strains, stress tensor components, and principal stresses will be computed accordingly. As in the results of the previous two cases, the first column images are for plane strain; the second column images are for plane stress; and the third column quantifies the delta between plane strain and plane stress solutions.

1. Displacement fields.

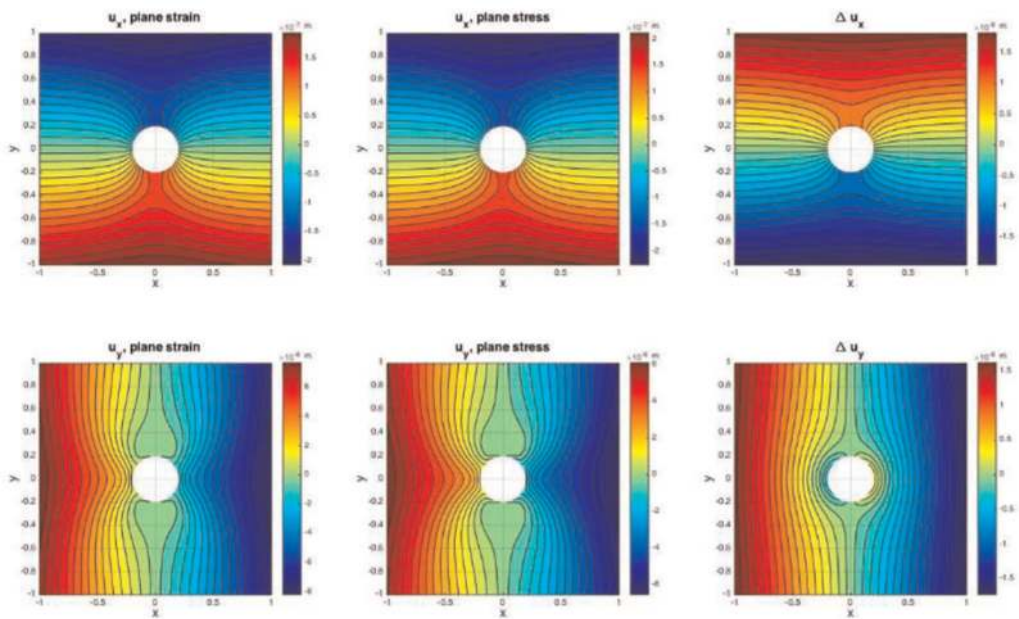


Figure C12.

The elastic displacement solutions around the single hole in an elastic plate subjected to both far-field stress and internal pressure. First column is for the plan strain solution, which is the sum of the results in the first column of **Figures C1** and **C7**. Second column is the plane stress solution, which is the sum of the results in the second column of **Figures C1** and **C7**. Third column quantifies the delta between plane stress and plane strain solutions. Since there is no displacement difference corresponding to the internal pressure effect, the deltas presented in the third column of this figure are identical to those in the third column of **Figures C1**.

2. Strain tensor components.

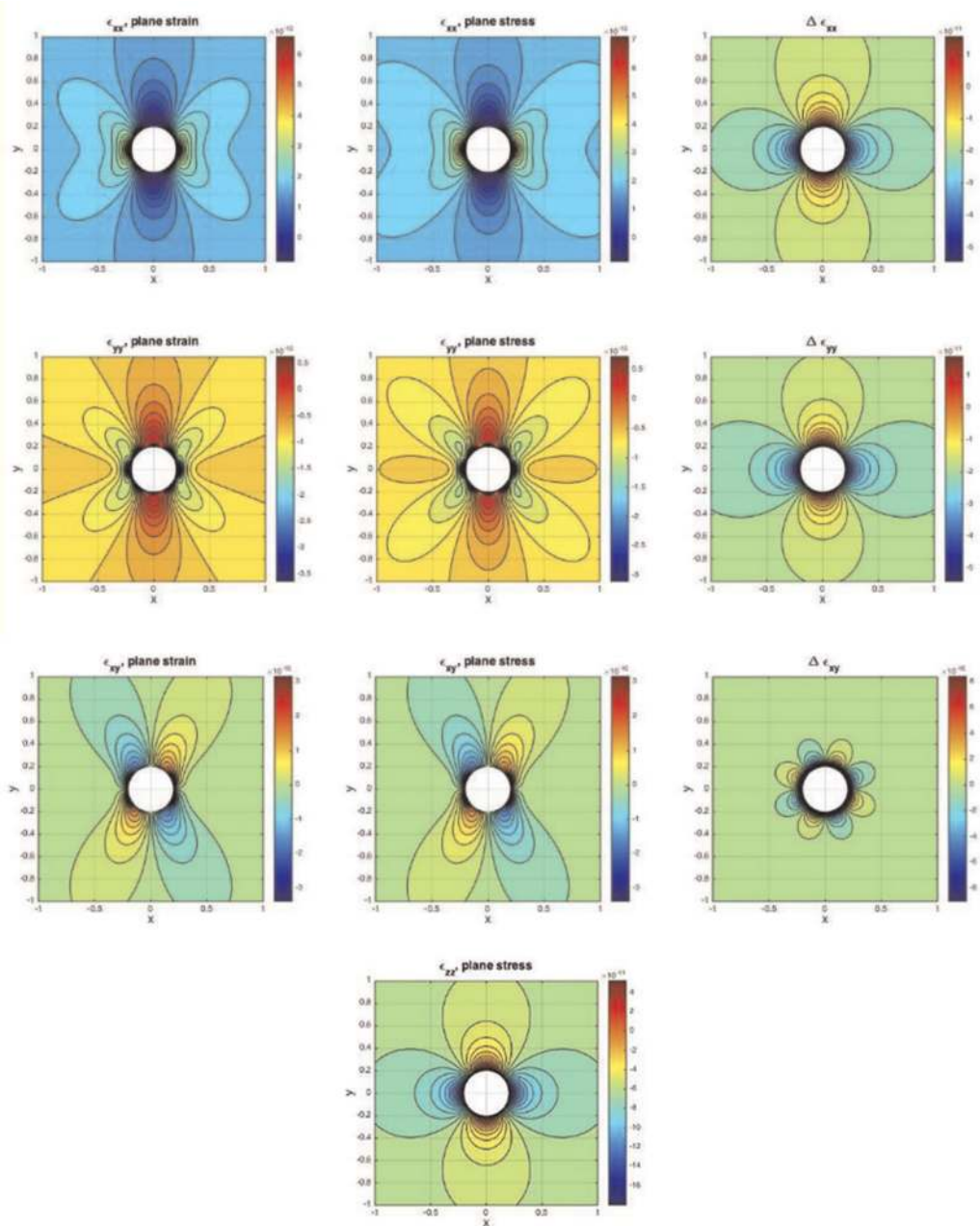


Figure C13. Strain tensor components around the single hole in an elastic plate subjected to both far-field stress and internal pressure. These solutions are obtained by analytical differentiation of the displacement components in Figure C12 in both x and y directions. $\epsilon_{zz} = 0$ for the plane strain solution and therefore there is no delta in z -direction.

3. Principal strains.

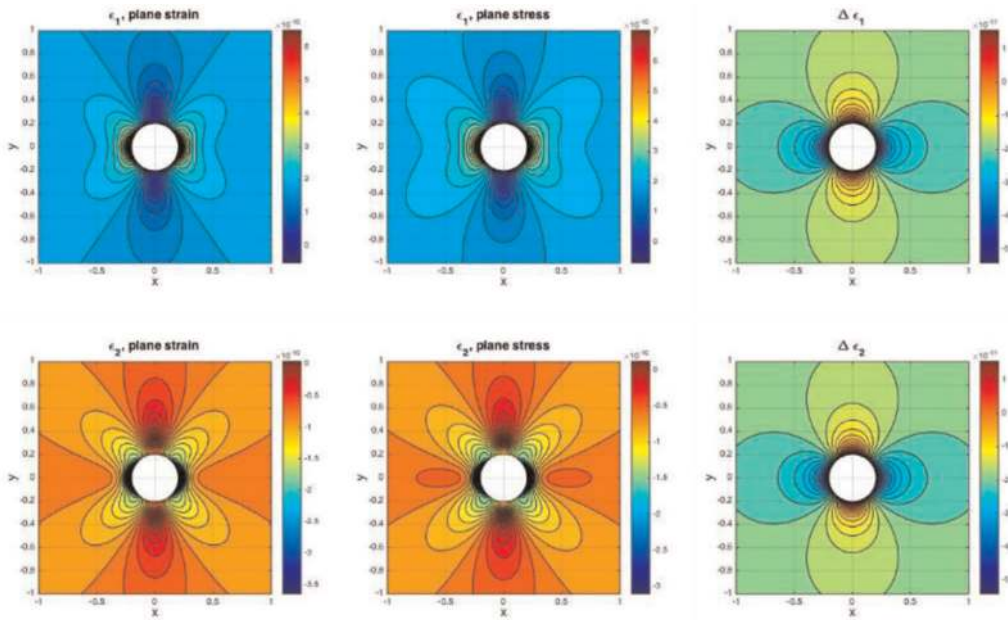


Figure C14. Principles strains around the single hole in an elastic plate subjected to both far-field stress and internal pressure. These solutions are obtained by applying Eq. (36) for the principal strain magnitude solution using the strain tensors in Figure C13.

4. Stress tensor components.

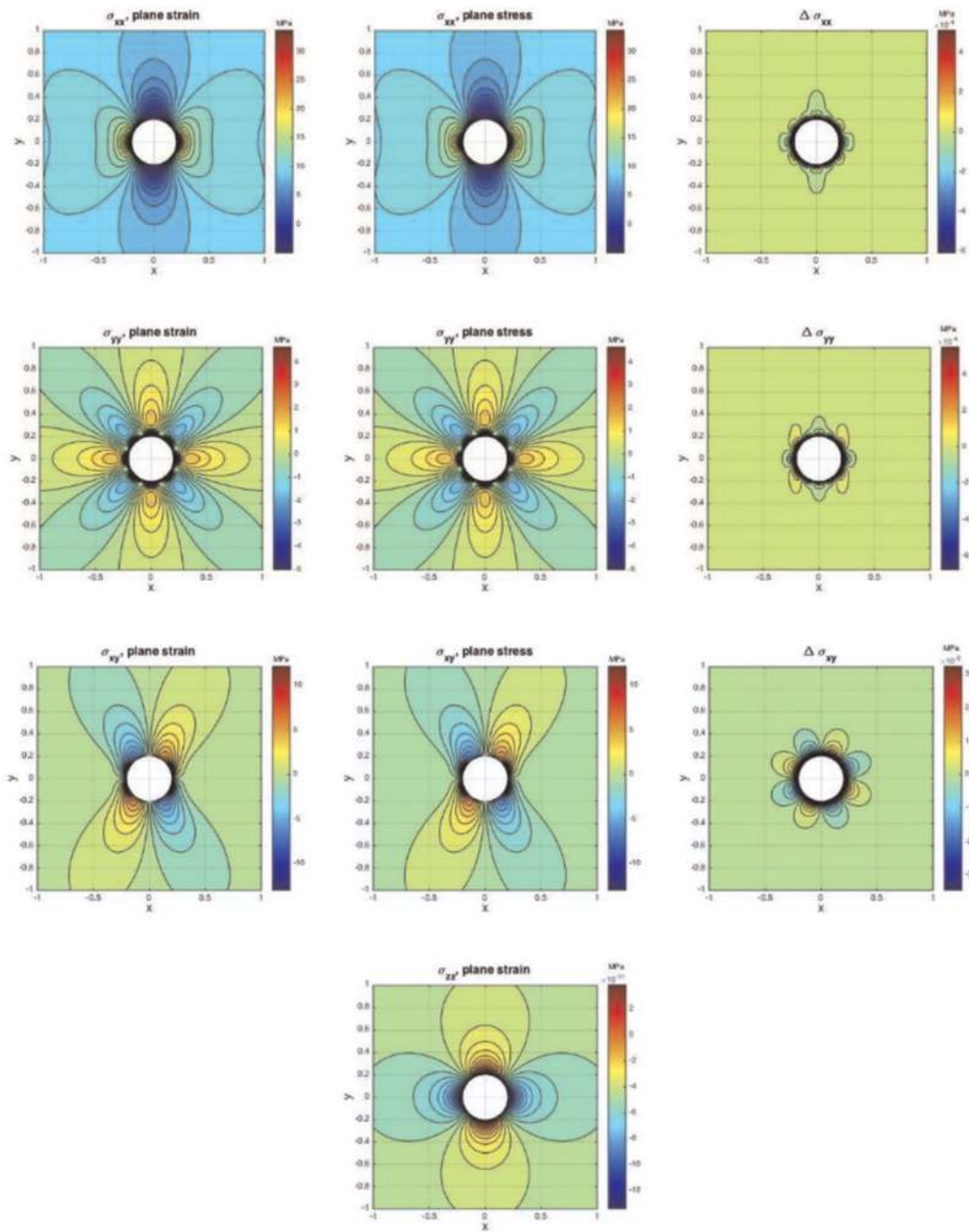


Figure C15.

Stress tensor components around the single hole in an elastic plate subjected to both far-field stress and internal pressure. These solutions are obtained from the relations between the strain tensor components and the stress tensor components shown in Eqs. (32)–(34). Note that $\sigma_{zz} = 0$ for plane stress solution and therefore there is no delta in the z -direction.

5. Principal stress.

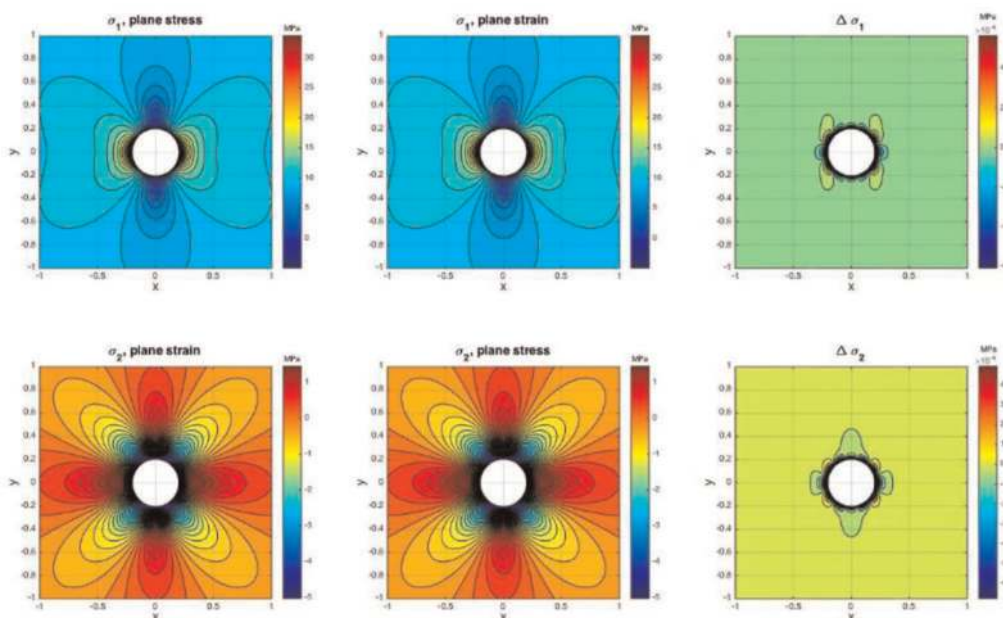


Figure C16. Principal stresses around the single hole in an elastic plate subjected to both far-field stress and internal pressure. These solutions are obtained by applying Eqs. (37) and (38) using the tensor stress components in Figure C15.

D. Multi-hole analysis: 5-hole problem (Case 2-1)

Comprehensive results are given here for the vector displacement fields, strain tensor components, principal strains, stress tensor components, and principal stresses for the elastic plate model represented in Case 2-1 with 5-holes subjected to far-field stress. The model input parameters are as given in Table 2. The first column images are for plane strain; the second column images are for plane stress; and the third column quantifies the delta between plane strain and plane stress solutions.

1. Displacement fields.

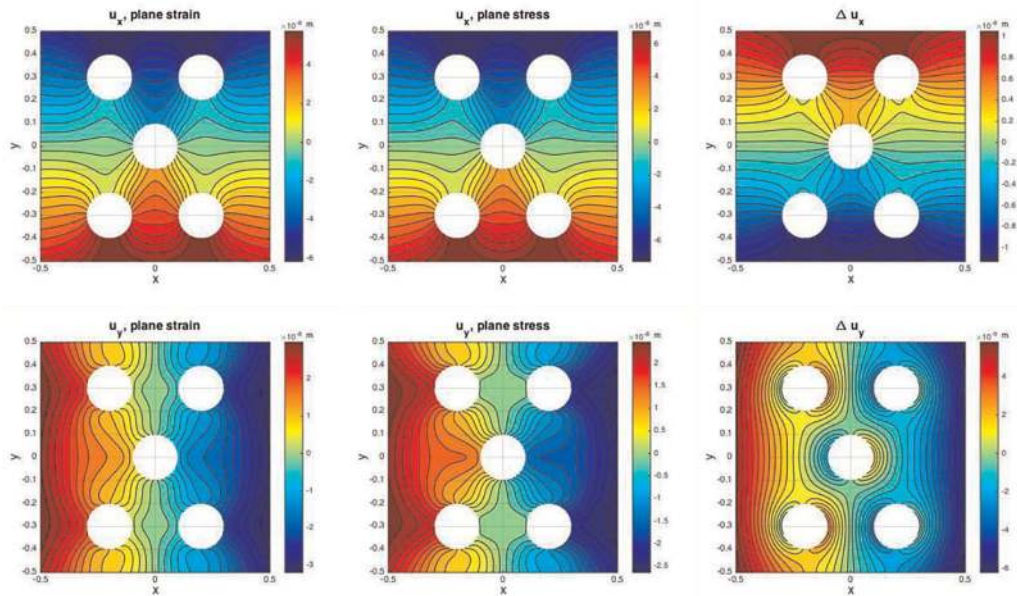


Figure D1.

Complete results of the elastic displacement solutions around 5-holes with equal radii ($r = 0.1$) in an elastic plate subjected to far-field stress. First column is for the plan strain solution given by Eqs. (15) and (16) for each single hole and then use Eqs. (23) and (24) to compute the total displacement vectors ($u_{x,\text{total}}$ and $u_{y,\text{total}}$) due to all holes combined. Second column is the plane stress solution given by Eqs. (17) and (18) and, similarly, using Eqs. (23) and (24) to compute the total displacement vectors due to all holes combined. Third column quantifies the delta (difference) between plane strain and plane stress solutions using Eqs. (25) and (26). Input parameters for this model are listed in Table 2.

2. Strain tensor components.

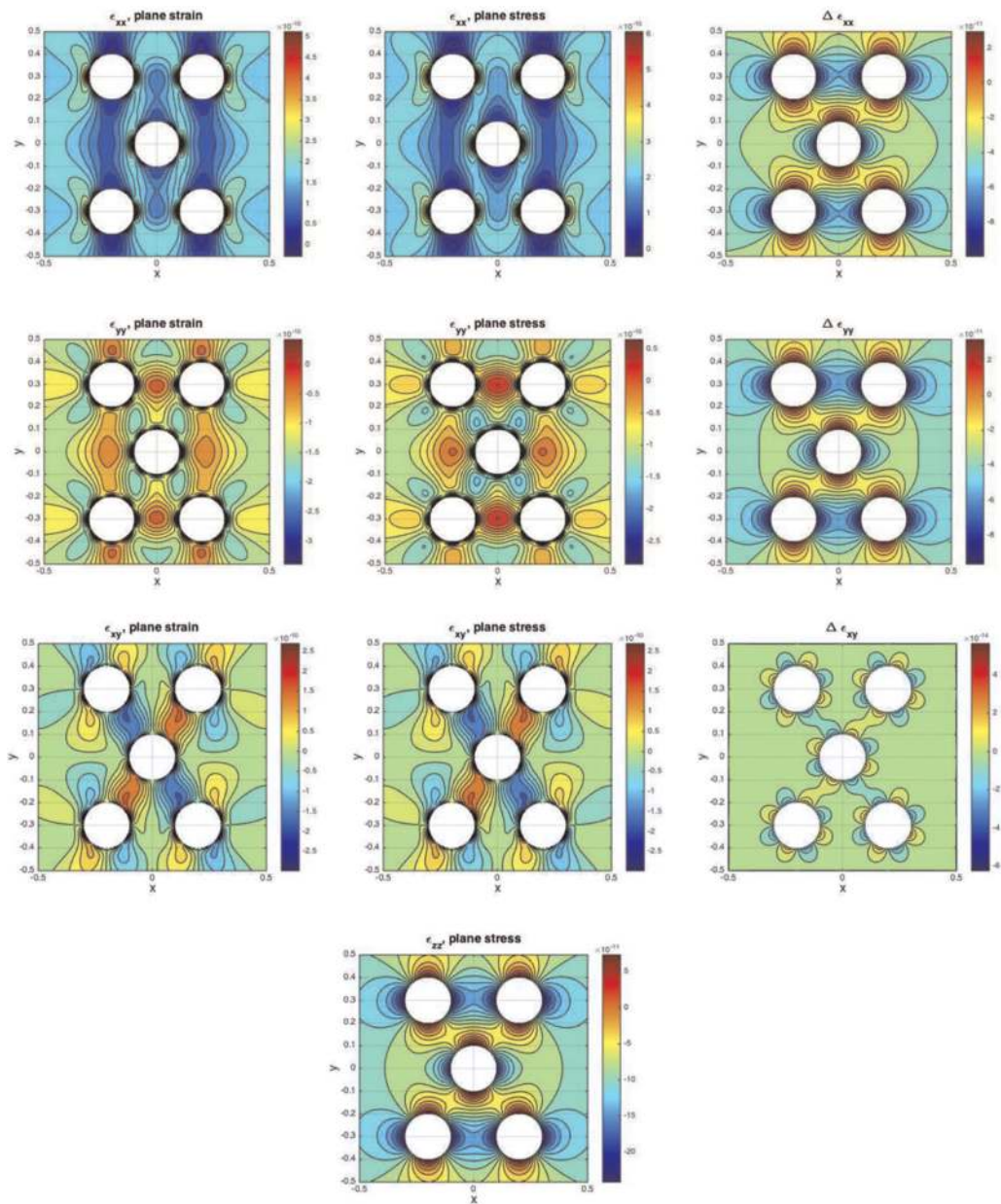


Figure D2.

Strain tensor components around 5-holes with equal radii ($r = 0.1$) in an elastic plate subjected to far-field stress. First column is for the plan strain solution. Second column is the plane stress solution. Third column quantifies the delta (difference) between plane strain and plane stress solutions. These solutions are obtained by analytical differentiation of the displacement components in **Figure D1** in both x and y directions. Since $\epsilon_{zz} = 0$ for the plane strain solution there is no delta in z -direction.

3. Principal strains.

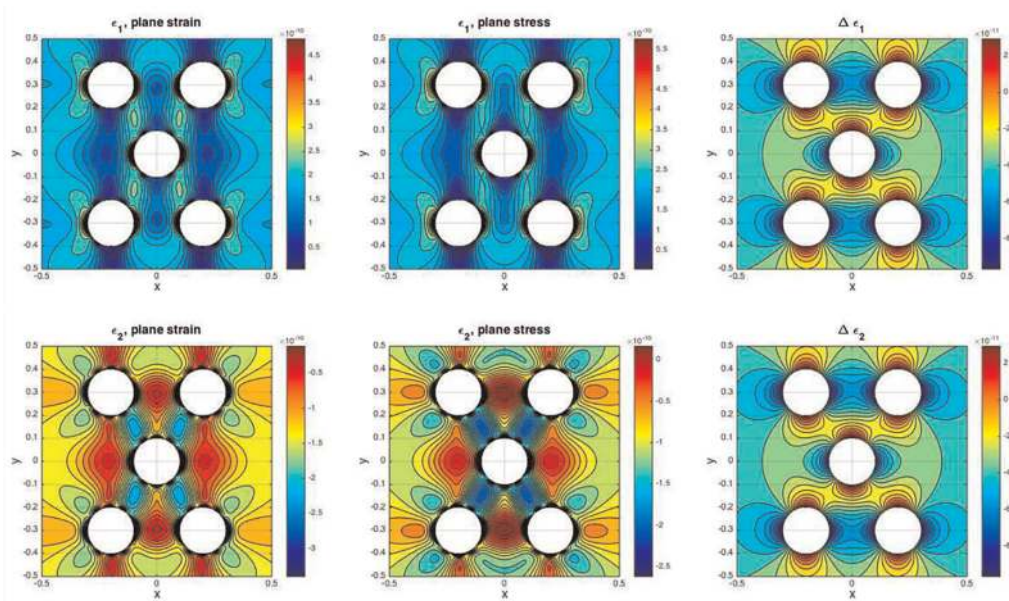


Figure D3.

Principles strains around 5-holes with equal radii ($r = 0.1$) in an elastic plate subjected to far-field stress. These solutions are obtained by applying Eq. (36) for the principal strain magnitude solution using the strain tensors in **Figure D2**.

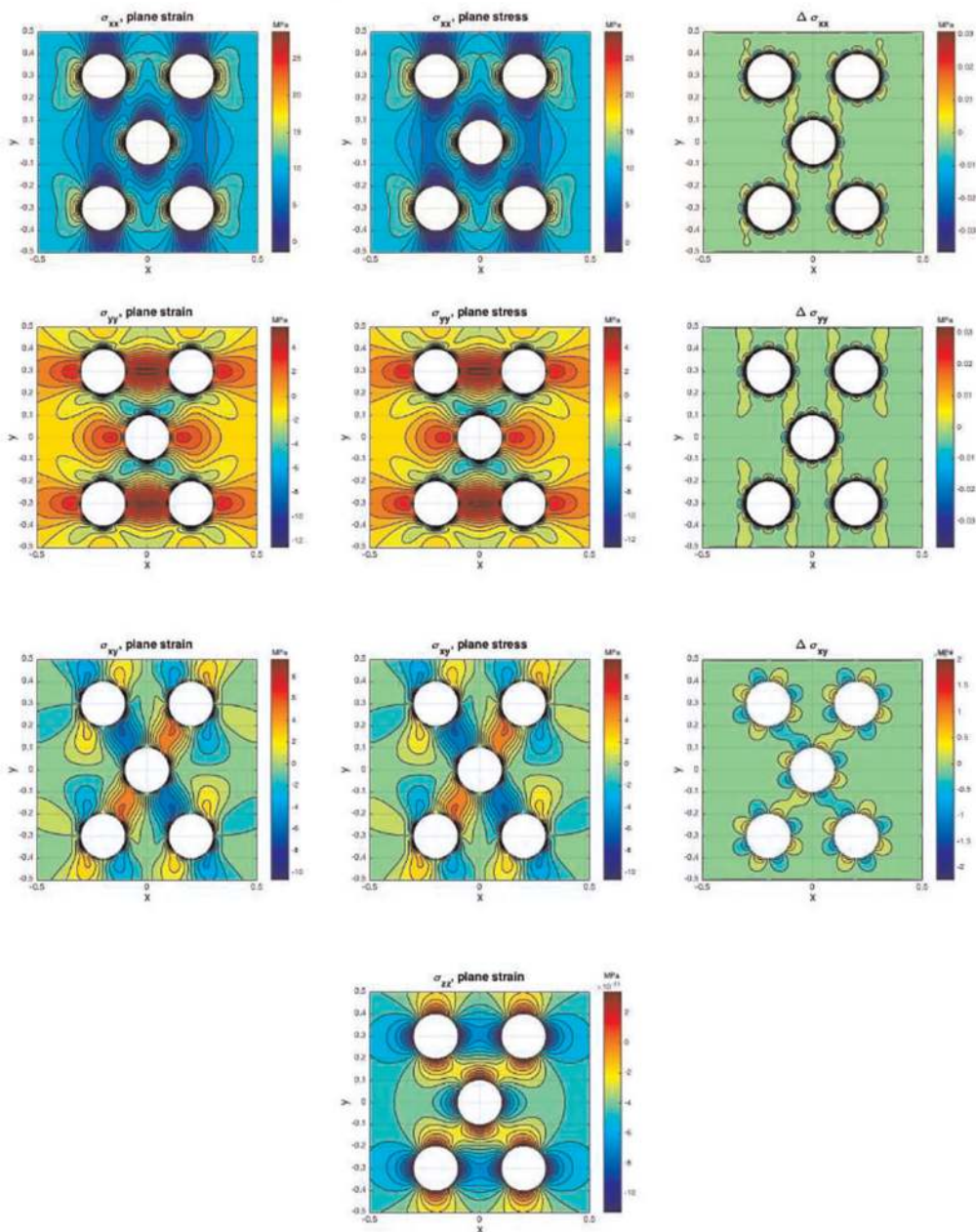


Figure D4. Stress tensor components around 5-holes with equal radii ($r = 0.1$) in an elastic plate subjected to far-field stress. These solutions are obtained from the relations between the strain tensor components and the stress tensor components shown in Eqs. (32)–(34). Since $\sigma_{zz} = 0$ for plane stress solution there is no delta in the z -direction.

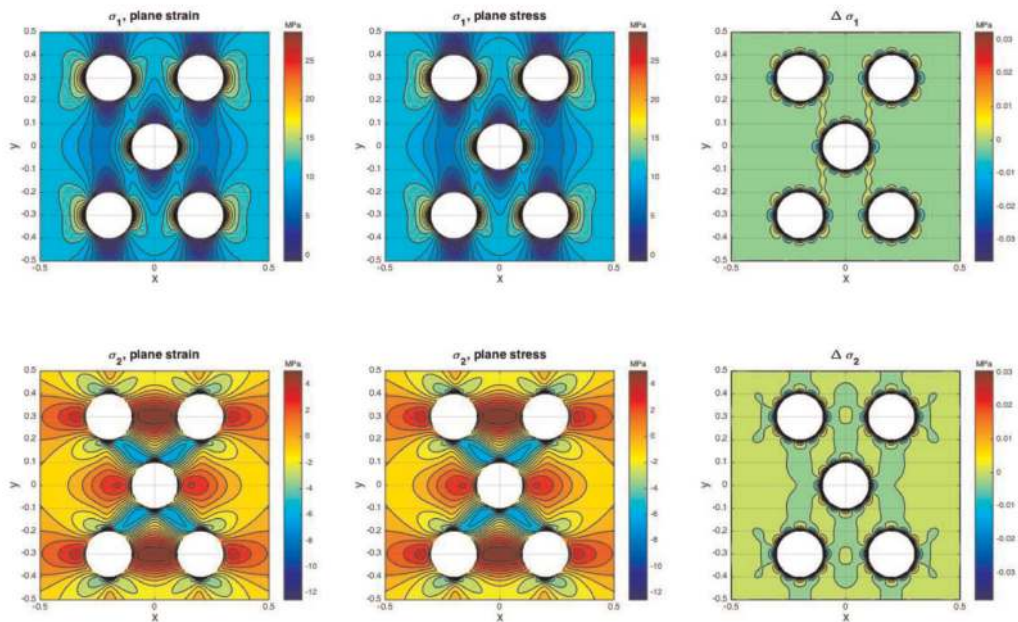


Figure D5. Principal stresses around 5-holes with equal radii ($r = 0.1$) in an elastic plate subjected to far-field stress. These solutions are obtained by applying Eqs. (37) and (38) using the tensor stress components in **Figure D4**.

4. Stress tensor components.
 5. Principal stresses.
- See (**Figure D5**).

Author details

Manal Alotaibi^{1,3} and Ruud Weijermars^{2,3*}


1 Department of Mathematics, College of Computing and Mathematics, KFUPM - King Fahd University of Petroleum and Minerals, Dhahran, Saudi Arabia

2 Department of Petroleum Engineering, College of Petroleum Engineering and Geosciences (CPG), KFUPM- King Fahd University of Petroleum and Minerals, Dhahran, Saudi Arabia

3 Center for Integrative Petroleum Research (CIPR), KFUPM - Dhahran, Saudi Arabia

*Address all correspondence to: ruud.weijermars@kfupm.edu.sa

IntechOpen

© 2022 The Author(s). Licensee IntechOpen. This chapter is distributed under the terms of the Creative Commons Attribution License (<http://creativecommons.org/licenses/by/3.0>), which permits unrestricted use, distribution, and reproduction in any medium, provided the original work is properly cited. 

References

- [1] Kirsch C. Die theorie der elastizitat und die bedurfnisse der festigkeitslehre. Zeitschrift des Vereines Deutscher Ingenieure. 1898;**42**:797-807
- [2] Thomas N, Weijermars R. Comprehensive atlas of stress trajectory patterns and stress magnitudes around cylindrical holes in rock bodies for geoscientific and geotechnical applications. Earth-Science Reviews. 2018;**179**:303-371
- [3] Weijermars R, Pham T, Etehad M. Linear superposition method (LSM) for solving stress tensor fields and displacement vector fields: Application to multiple pressure-loaded circular holes in an elastic plate with far-field stress. Applied Mathematics and Computation. 2020a;**381**:125234. DOI: 10.1016/j.amc.2020.125234
- [4] Weijermars R, Wang J, Nelson R. Stress concentrations and failure modes in horizontal wells accounting for elastic anisotropy of shale formations. Earth-Science Reviews. 2020b;**200**:102957. DOI: 10.1016/j.earscirev.2019.102957
- [5] Aadnoy BS, Looyeh R. Petroleum Rock Mechanics: Drilling Operations and Well Design. Boston: Gulf Professional Publishing; 2012. DOI: 10.1016/C2009-0-64677-8
- [6] Fjaer E, Holt RM, Horsrud P, Raaen AM. Petroleum Related Rock Mechanics. 2nd ed. Elsevier; 2008
- [7] Jaeger JC, Cook NG, Zimmermann RW. Fundamentals of Rock Mechanics. 4th ed. John Wiley & Sons; 12 March 2009. pp. 475
- [8] Weijermars R. Stress cages and fracture cages in stress trajectory models of wellbores: Implications for pressure management during drilling and hydraulic fracturing. Journal of Natural Gas Science and Engineering. 2016;**36**:986-1003
- [9] Wang J, Weijermars R. Expansion of horizontal wellbore stability model for elastically anisotropic shale formations with anisotropic failure criteria: Permian Basin case study. In: 53rd US Rock Mechanics/Geomechanics Symposium. OnePetro; 2019
- [10] Koslowska B. Experimental investigations of elastic-plastic strain states on various stages of material plastifying. Journal of Theoretical and Applied Mechanics. 2016;**54**(2):489-501. DOI: 10.15632/jtam-pl.54.2.489
- [11] Yi W, Rao Q, Ma W, Sun D, Shen Q. A new analytical-numerical method for calculating interacting stresses of a multi-hole problem under both remote and arbitrary surface stresses. Applied Mathematics and Mechanics. 2020; **41**(10):1539-1560
- [12] Green AE, Taylor GI. Stress systems in aeolotropic plates, III. Proceedings of the Royal Society of London. Series a. Mathematical and Physical Sciences. 1945;**184**(997):181-195
- [13] Clark RA. Three-dimensional corrections for a plane stress problem. International journal of solids and structures. 1985;**21**(1):3-10
- [14] Green AE. Three-dimesnional stress systems in isotropic plates. I. Philosophical transactions of the Royal Society of London. Series A, Mathematical and Physical Sciences. 1948;**240**(825):561-597
- [15] Yang Z, Hou J, Wang GY, Xiong ZH. The stress and strain concentrations associated with two interacting holes in a finite thickness elastic plate subjected to

tensile stress. In: Key Engineering Materials. 2011;462:48-53 Trans Tech Publications Ltd

[16] Filon LN. On an approximate solution for the bending of a beam of rectangular cross-section under any system of load, with special reference to points of concentrated or discontinuous loading. Philosophical transactions of the Royal Society of London. Series A, Containing Papers of a Mathematical or Physical Character. 1903;201(331-345):63-155

[17] Jaeger JG, Cook NGW. Fundamentals of Rock Mechanics. 3rd ed. London: Chapman & Hall; 1979

[18] Goodman RE. Introduction to Rock Mechanics. Vol. 2. New York: Wiley; 1989 Jan 17

[19] Jussila P. Analytical solutions of the mechanical behaviour of rock with applications to a repository for spent nuclear fuel. 1979. <https://www.osti.gov/etdweb/biblio/599095>

[20] Brady BHG, Brown ET. Rock Mechanics for Underground Mining. 3rd ed. Dordrecht: Kluwer Academic Publishers; 2005

[21] Valkó P, Economides MJ. Hydraulic Fracture Mechanics. Chichester: Wiley; 1995

[22] Saada AS. Elasticity Theory and Applications. 2nd ed. Malabar, Florida: Krieger Publishing Company; 1993

[23] Lamé G. Leçons sur la théorie mathématique de l'élasticité des corps solides. Paris: Bachelier; 1852

[24] Green AE. General bi-harmonic analysis for a plate containing circular holes. Proceedings of the Royal Society of London. Series a. Mathematical and Physical Sciences. 1940;176(964):121-139

[25] Ling CB. On the stresses in a plate containing two circular holes. Journal of Applied Physics. 1948;19(1):77-82

[26] Haddon RA. Stresses in an infinite plate with two unequal circular holes. The Quarterly Journal of Mechanics and Applied Mathematics. 1967;20(3):277-291

[27] Kooi CB, Verruijt A. Interaction of circular holes in an infinite elastic medium. Tunnelling and Underground Space Technology. 2001;16(1):59-62

[28] Wang J, Crouch SL, Mogilevskaya SG. A complex boundary integral method for multiple circular holes in an infinite plane. Engineering Analysis with Boundary Elements. 2003;27(8):789-802

[29] Weijermars R, Wang J, Pham T. Borehole failure mechanisms in naturally fractured formations. Rock Mechanics and Rock Engineering. May 2022;55(5):3001-3022

[30] Weijermars R, Ettehad M. Displacement field potentials for deformation in elastic media: Theory and application to pressure-loaded boreholes. Applied Mathematics and Computation. 2019;340:276-295

[31] Meguid SA, Shen CL. On the elastic fields of interacting defected and main hole systems. International Journal of Mechanical Sciences. 1992;34(1):17-29

[32] Nádai A, Hodge PG Jr. Theory of Flow and Fracture of Solids. Vol. II. New York, NY: McGraw-Hill Book Company Incorporated; 1963